A Three-Port DC/DC Converter (TPC) for Small-Scale Standalone PV-Battery Systems

by

Ahmed Mahmood Ghazi Mahmood Bakhairiba

A thesis

presented to the University of Waterloo

in fulfillment of the

thesis requirement for the degree of

Master of Applied Science

in

Electrical and Computer Engineering

Waterloo, Ontario, Canada, 2023

Author’s Declaration

I hereby declare that I am the sole author of this thesis. This is a true copy of the thesis, including any required final revisions, as accepted by my examiners.

I understand that my thesis may be made electronically available to the public.

Abstract

While conventional electricity generation relies on fossil fuels like coal, oil, and gas, renewable energy relies on abundant sources like sunlight, wind, water, and geothermal heat, offering eco-friendly alternatives with minimal emissions. Unlike conventional electricity generation, renewable sources reduce our carbon footprint, aid in combating climate change, and provide lasting energy security. Due to their intermittent nature, implementing energy storage and smart grid technologies becomes essential to maintain a stable electricity supply.

Off-grid communities face challenges in accessing reliable energy due to lack of connection to centralized grids. Therefore, renewable energy sources, such as solar, wind, and other sources can help these communities establish self-sustaining, clean, and cost-effective power solutions. Despite the impressive advancements in renewable energy technologies, a significant global population still lacks access to basic energy. According to the United Nations, their ambitious objective is achieving universal energy access, aiming for 100% global coverage by 2030.

Therefore, this thesis provides a solution for off-grid communities who lack energy access. It proposes a novel design of a three-port DC/DC Converter (TPC) for small-scale standalone PV-Battery applications. The derivation process of the topology and the optimization methodology are comprehensively explained. Moreover, the modes of operation are elaborated to demonstrate the functionality of the TPC. Furthermore, the controlling method to regulate the output voltage, control the battery current, and track the maximum power point (MPP) of the PV source is discussed.

The performance of the proposed topology is validated using PSIM software. A comprehensive simulation analysis is conducted for a load profile of an induvial household in Zimbabwe over a 24-hour period. The steady-state waveforms for all the modes and the mode transition waveforms are all presented and discussed. Additionally, the efficiency for the proposed design is calculated for different range of loads and compared with other topologies. Finally, two case studies are given to observe and analyze the system's response to different scenarios during the 24-hour period.

Acknowledgments

First of all, I would like to express my deepest thanks and gratitude to my supervisor, Professor. Mehrdad Kazerani. Without his continued guidance, invaluable advice, deep insight, and support during my MASc journey at the University of Waterloo, this thesis project could not have come anywhere close to this. I am very happy to have had the chance to learn, experience and try many aspects of academic and practical life during this time. His thoughts, encouragement and trust have been inspiring countless times.

I would like to Thank Professors Magdi Salama and Ramadan El-Shatshat for their invaluable service as my thesis readers. Their expertise and insightful feedback significantly enhanced the quality of my research and thesis. I am grateful for their dedication and commitment to guiding me through this academic endeavor.

I would like to extend my sincere gratitude to my esteemed colleagues and friends, Nasrin Einabadi and Miswar A. Syed, for their invaluable assistance and unwavering support. I have greatly benefited from their expertise and guidance.

I would like to express my heartfelt thanks to my dear friends, Saleh Ba Raean, Tamam Baashn, and Mohammed Alkatheri, for their unwavering love and continuous support. Their friendship has been a constant source of strength and comfort in my life, and I am truly blessed to have them by my side.

With great appreciation, I acknowledge HOUSE OF INVENTION headed by Sheikh Abdullah Bugshan for granting me the scholarship and giving me the opportunity to enhance my experience and education.

Dedication

This is dedicated to:

- My great beloved parents, who never stop giving of themselves in countless ways.

- My beloved brothers and sisters, whom I cannot find a replacement for.

- All my family, the symbol of love and giving.

- My friends who encourage and support me.

- All the people in my life who touch my heart.

Table of Contents

List of Figures

List of Tables

List of Abbreviations

TPC	Three-Port Converter
MPC	Multi-Port Converter
ESS	Energy Storage System
DIC	Dual-Input Converter
SEPIC	Single-Ended Primary Inductor Converter
MPP	Maximum Power Point
SoC	State of Charge
MPPT	Maximum Power Point Tracking
DO	Dual-Output
DI	Dual-Input
SISO	Single-Input Single-Output
P&O	Perturb and Observe
PI	Proportional-Integral
PV2B	PV-to-Battery
PV2L	PV-to-Load
B2L	Battery-to-Load
PV&B2L	PV-and-Battery-to-Load
PV2B&L	PV-to-Battery-and-Load

Chapter 1
Introduction

Conventional electricity generation depends primarily on fossil fuels, such as coal, oil, and natural gas, which have been the cornerstone of worldwide energy production for many years. While conventional electricity generation has ensured a reliable and accessible energy source, it also presents notable environmental and sustainability concerns. The combustion of these fuels releases significant quantities of carbon dioxide and other greenhouse gases into the atmosphere. This results in the formation of a dense layer that traps heat, causing a rise in Earth's temperatures. As the world moves towards cleaner and more sustainable energy solutions, the drawbacks and adverse effects of conventional electricity generation highlight the critical necessity to transition towards renewable and low-carbon sources. This shift is imperative to ensure an environmentally responsible energy future.

While conventional electricity generation depends on finite fossil fuels, renewable energy utilizes plentiful and replenishable natural resources sources such as sunlight, wind, water, and geothermal heat. These sustainable sources provide environmentally friendly alternatives, emitting minimal to no pollutants or greenhouse gases, thus decreasing our carbon footprint and contributing to the fight against climate change. Additionally, their sustainable attributes ensure lasting energy security, reduce reliance on finite fuels, fosters new job opportunities, and aligns with the broader objective of nurturing a greener and healthier planet.

Renewable energy technologies, such as solar panels and wind turbines, have seen impressive advancements, resulting in increased efficiency and broader accessibility. With solar panels becoming increasingly adept at harnessing sunlight and wind turbines being optimized for maximal energy generation, the prospect of reducing our reliance on conventional electricity generation becomes even more promising. Despite the environmental advantages of renewable energies, these sources encounter challenges by their intermittent nature because of their reliance on sunlight and wind speed, which results in energy production fluctuations. This issue underscores the necessity for solutions like energy storage and smart grids to ensure a stable electricity supply. With the increasing demand for sustainable energy, it becomes crucial to find effective ways for managing and balancing the fluctuating characteristics of renewable sources. Advancements in storage and grid management are essential for realizing the full potential of renewable energies and guaranteeing a reliable and resilient energy future.

Off-grid communities, often located in remote or underserved regions, encounter significant difficulties in obtaining reliable energy sources. The lack of connection to centralized electricity grids can hinder socio-economic progress, education, healthcare, and communication. These communities often resort to inefficient and environmentally detrimental alternatives such as diesel generators or traditional biomass to fulfill their energy requirements. However, advancements in renewable energy technologies, combined with the adoption of microgrids and decentralized energy systems, are revolutionizing energy accessibility for these underserved and marginalized populations. Through the utilization of solar, wind, and other renewable sources, off-grid communities can establish self-sustaining energy solutions that deliver clean, cost-effective, and consistent power. This not only enhances the overall quality of life and economic opportunities for residents but also contributes to environmental conservation by reducing reliance on polluting energy sources.

1.1 Motivation

While economically advanced countries are celebrating their technological advancements in utilizing clean and renewable energy sources, a significant segment of the global population continues to struggle for the basic right to access energy. As per the 2020 World Energy Outlook by International Energy Access (IEA), approximately 771 million individuals around the world continue to lack access to electricity [1]. A notable proportion of people deprived of energy access is predominantly found in African nations, particularly Sub-Saharan Africa, developing countries in Asia, Pacific islands, Latin America, and some Middle Eastern countries [1]. These communities are poor, situated in remote regions with challenging landscapes, or located on clusters of small islands where the establishment of a central power grid is either nonexistent or economically impractical.

The developed nations have been successful in extending energy access to their remote communities due to their robust grid infrastructure, strong economic conditions, and heightened awareness. Although their success rate is notable, the incorporation of various distributed energy resources into the traditional grid, all while upholding supply security and ensuring stable grid operation, has presented challenges for the system operator. However, the obstacles encountered by developing countries are notably more severe and intricate, posing a substantial hindrance to enhancing energy access for these communities. Poverty, malnutrition, illiteracy, poor living, and environmental conditions have been identified as interconnected factors associated with deprived energy access. This creates an unending cycle that

hinders the progress of individuals and, ultimately, the entire community. In remote communities, Diesel Generator sets have gained popularity as an energy source, contributing to improved electricity access. Nonetheless, escalating costs and challenges associated with fuel transportation have cast doubts about affordability and ease of access. Additionally, high maintenance expenses and negative environmental effects have compounded the existing problems.

Alongside these existing challenges, the task of establishing clean and self-sustaining energy sources presents further complexities. Recognizing these concerns, international entities such as the United Nations, World Bank, local governments, and voluntary organizations have played an active role in deliberating, supporting, and executing diverse energy access initiatives aligned with specific regional or national objectives. The United Nations Secretary-General's Advisory Group on Energy and Climate Change has outlined an ambitious objective of achieving universal energy access, aiming for 100% global coverage [2]. Although there has been a positive trend in energy accessibility, rising from 71% in 1990 to 87% in 2016, and subsequently reaching 89.6% in 2018 [1], this growth rate falls insufficient in achieving the universal energy access by 2030.

1.2 Research Objectives

The primary goal of this thesis is to develop a three-port DC/DC Converter (TPC) for small-scale standalone PV-Battery applications. The outcome of this research will benefit underserved populations who reside in off-grid communities. The objective is to satisfy the requirements of the load on an instantaneous basis while respecting the limitations on the renewable energy source (PV source), energy storage system (battery), and system components, as well as the requirements on the quality of power received by the load.

Key design features include: (i) cost-effectiveness, achieved by minimizing the components count and maximizing the components sharing among different conversions withing the TPC; (ii) reliability, ensuring robust operation throughout a full 24-hour period despite load and solar fluctuations; and (iii) dual output voltage, attained by offering two output voltage levels (12V & 48V) within the TPC.

1.3 Organization of the Thesis

The structure of this thesis is organized as follows:

Chapter 2 provides an overview of traditional hybrid DC energy systems and their core components. It also includes a comprehensive literature review on Three-port Converters (TPCs).

Chapter 3 delves into the design of the TPC. It encompasses the derivation of the topology, the modes of operation, the system specifications, and the description of the control unit.

Chapter 4 offers an in-depth simulation analysis conducted using the PSIM software. It gives the simulation results for the modes of operation and the mode transition during operation. Furthermore, the efficiency of the design is presented for different range of loads. Finally, two case studies over a 24-hour period are simulated to observe and analyze the system's response.

Chapter 5 presents the conclusions for this thesis and the recommendations for future work.

Chapter 2
Background and Literature Review

2.1 Hybrid Energy Systems

In traditional hybrid DC energy systems, multiple input sources deliver electrical energy to the dc link through unidirectional single-input single-output (SISO) converters [3], as shown in Figure 2.1. Due to the intermittent nature of some input sources, such PV and wind sources, energy storage systems (ESS) are incorporated in the system be connecting them to the DC link through bidirectional DC/DC converters to store surplus energy and deliver deficit energy when needed. Furthermore, various loads are connected to the DC link either directly or via DC/DC converters. Incorporating a significant number of DC/DC converters leads to a complex design, low power density, and substantial cost.

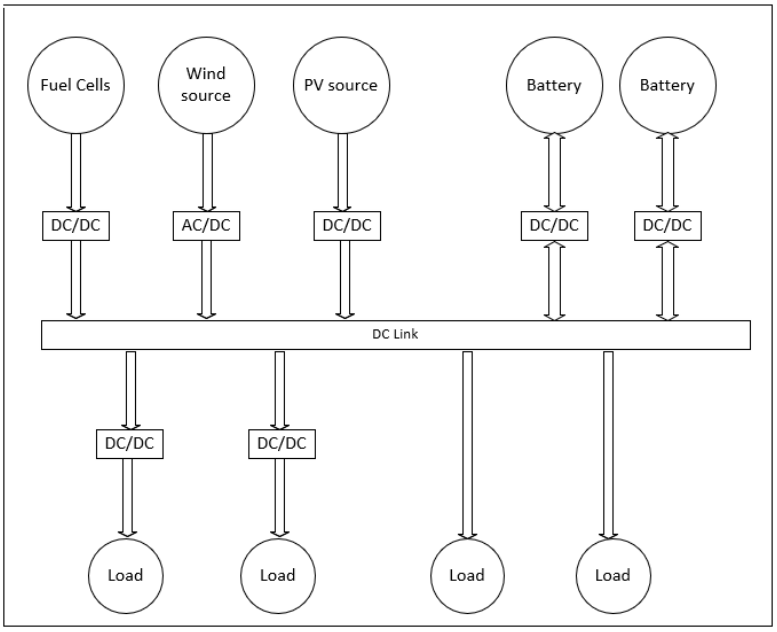

Figure 2.1: Traditional Hybrid DC Energy System

To overcome the disadvantages, it is necessary to reduce the design complexity and number of power conversion stages and integrate these multiple SISO converters into a Multi-Port Converter (MPC) that features high power density and low cost [4]. The simplest form of these MPCs is the Three-Port Converter (TPC) which consists of an input port to connect a PV panel, a bidirectional port to connect an ESS, and a unidirectional port for connecting a load.

2.2 Three Port Converters

The research interest in TPCs has been growing. TPCs, as shown in Figure 2.2, show significant advantages over hybrid DC energy systems because of their lower number of power conversion stages, higher efficiency, and compact size [5],[6]. Furthermore, some circuit components such as semiconductor switches and passive elements can be multiplexed to decrease the number of components and enhance power density. Because of these notable advantages, many TPCs have been proposed, studied, designed, and implemented for different applications, such as stand-alone renewable power system [7]-[9], distributed renewable power system [10], microgrid power system [11], and fuel-cell power system [12],[13].

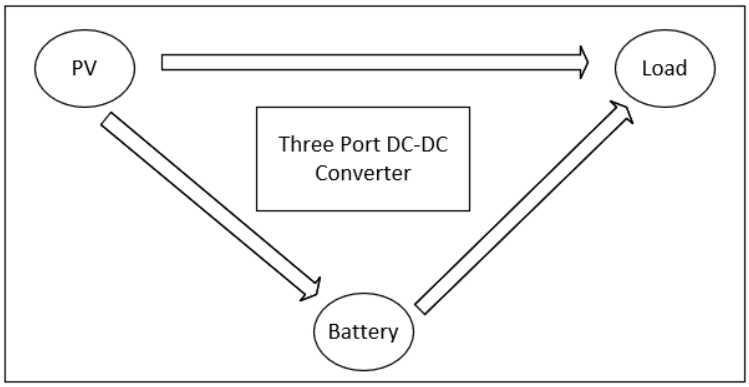

Figure 2.2: Three Port Converter (TPC)

A fully-isolated DC/DC TPCs can be constructed using magnetic coupling provided by a high-frequency transformer [12],[14]. Since each input port requires one independent inductor, this family of TPCs is bulky. If isolation is not a requirement, non-isolated TPCs are more efficient due to the absence of the transformer parasitic losses and leakage inductance [15]. Moreover, non-isolated TPCs, in contrast to isolated TPCs, feature compact design and high-power density [15].

In the most basic form, in a non-isolated DC-DC TPC, power conversions are accomplished by combining two independent DC/DC converters through a shared DC bus [16]-[18]. The typical configuration of a non-isolated TPC consists of a unidirectional DC/DC converter and a bidirectional DC/DC converter, as shown in Figure 2.3. This configuration is used in many applications [17],[18]. However, a high degree of integration is not achieved because very few devices are multiplexed, and the topology suffers extra losses from multiple power conversion stages.

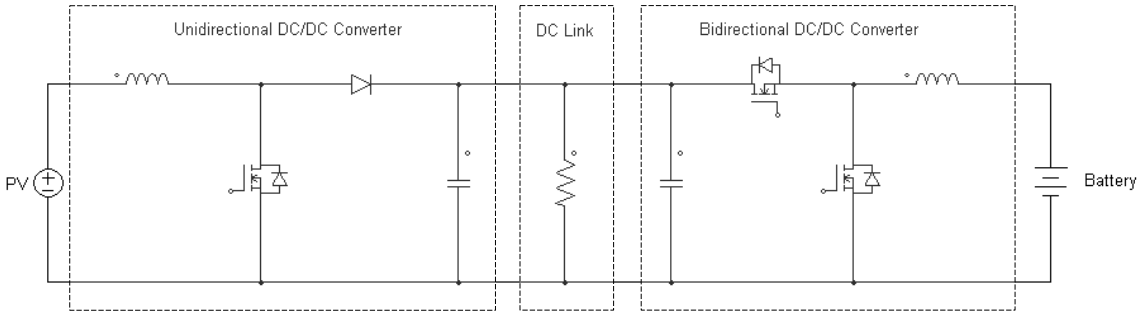

Figure 2.3: The Traditional configuration of a three port Converters

In [19]-[23], authors researched and presented multiple-input converter designs, featuring high degree of integration and high-power density. However, the paths in these multiple-input converters are unidirectional, and consequently they are not suitable for applications involving bidirectional ESS elements.

In [24], a systematic approach to derive non-isolated DC-DC TPCs from dual-input converters (DIC) and dual-output converters (DOC) is proposed. Then, a demonstration for the proposed derivation method is given by building a TPC based on the conventional boost converter. The design features low component count, due to utilizing three switches, three diodes, and only a single inductor. This makes the design cost effective and gives it high power density. Moreover, the efficiency of the design is very high compared with other TPC topologies proposed in the literature. However, this design requires a large capacitor across the battery to filter the pulsating current.

In [25], a topology derivation method for non-isolated DC-DC TPCs is proposed. Then a demonstration for the proposed derivation method is given by building a TPC based on the conventional buck converter. The design features low components count, and thus, low cost. However, the efficiency of the design is low compared with other TPC topologies proposed in the literature.

In [26], A non-isolated DC/DC TPC with minimum number of switches is proposed based on single-ended primary inductor converter (SEPIC). This topology features high voltage step-up with only two active switches. The output voltage is boosted to 380V from a 24V PV and 36V battery. However, the power density of this topology is low since it contains one single inductor as well as a coupled inductor. Also, this design doesn't allow the controller to track maximum power point (MPP) when charging the battery with a load connected to the DC bus.

In [27], a new non-isolated DC/DC TPC for off-grid solar-power applications, such as dc motor drives and LED drivers, is proposed. This topology features lower active component count (three

switches and only one diode). In addition, this design is reconfigurable and can work as a boost converter, a buck-boost converter, or a forward converter to support different scenarios. However, the ESS is not grounded, whereas grounding is preferred for safety purposes. Furthermore, the inductor in this topology is coupled which increases the power density and the cost of the system.

In [28], a new non-isolated DC/DC TPC that features soft switching and high efficiency is proposed. To achieve full soft switching, Auxiliary circuit components are used such as diodes and snubber capacitors. However, the design is very complex as the number of active and passive components becomes very large. The topology utilizes four switches, five diodes, and a coupled inductor. Therefore, the design is bulky, costly, and has low power density.

In [29], a non-isolated TPC design based on buck-boost topology is proposed for photovoltaic applications. Since the design is based on buck-boost converter, it features stepping the voltage up and down while maintaining a positive polarity voltage for the output port. It is mentioned that this design features high voltage gain, but it only boosts the voltage from 12V to 24V. Furthermore, four switches and two inductors were used to implement the circuit. The result was a design with a large design in weight and size.

In [30], a new non-isolated three input DC/DC converter for Hybrid PV/fuel cell (FC)/Battery Applications is proposed. The design is comprised of a conventional boost converter and a buck-boost converter. It features a high voltage gain since it can boost the voltage higher than a conventional boost converter. However, the number of components is high because it consists of four switches, four diodes and two inductors. Also, the efficiency is low compared with other TPC topologies proposed in the literature.

In [31], a developed structure of non-isolated DC/DC TPC is proposed. This design features high step-up voltage while maintaining low normalized peak inverse voltage on the switches/diodes. The proposed design shows its capability to increase the voltage gain compared with other topologies from the same category. However, the number of components needed to implement the circuit is higher than that for other proposed designs. It uses five switches, three diodes, and four inductors. Thus, this design is very bulky, costly and has low power density.

In [32], a new non-isolated DC/DC TPC topology is proposed by integrating two boost converters to achieve high voltage step-up capability. This design focuses on achieving soft switching by adding auxiliary circuits to reduce switching losses. Thus, this design shows a good overall efficiency.

However, they utilized a high number of active components: five diodes and four switches to implement this circuit. Furthermore, they needed to use two coupled inductors and many snubber capacitors. The result was a design that has low power density and is very costly.

In [33], a new design for Photovoltaic-Wind and Hybrid Energy Storage is integrated as multi-source DC/DC converter configuration for DC microgrid applications. The hybrid energy storage interfaces supercapacitor and battery to handle the fluctuations from the wind source. This design uses only three switches to control three input sources. However, they couldn't achieve a regulated voltage in all modes of operation. Also, the efficiency is not reported in the paper.

In [34], a novel non-isolated DC/DC TPC with high-voltage gain for stand-alone photovoltaic applications is proposed. This design features high step-up voltage capabilities by boosting a 24V PV and a 48V battery to a 400V output. However, they used a rather large number of components to achieve this boosted voltage. They used one coupled inductor, five diodes and three switches. Therefore, the design is bulky, costly, and has low power density.

In [35], a non-isolated DC/DC TPC is proposed for stand-alone PV/Battery applications. This converter features a high voltage gain and implements soft switching. Although, this converter does not utilize diodes, the power density is still low since five switches and two coupled inductors are used in the circuit. Thus, they ended up with a costly design with a large volume and weight.

In [36], a non-isolated DC/DC TPC for hybrid energy systems is proposed. This design features high voltage step-up capability and uses resonant auxiliary circuits to provide soft switching condition for the switches. However, the number of components is high (five diodes and three switches). Furthermore, a coupled inductor was used to boost the voltage. As a result, the design volume and overall cost increased.

To facilitate comparison of topologies, specific criteria have been established, taking into account various factors. Additionally, weights have been allocated to each criterion, considering the specific needs of the target application, which is aimed at individuals residing in off-grid communities, particularly in sub-Saharan Africa. For example, a weight of '5' has been assigned to the cost criterion, reflecting the financial constraints faced by most individuals in off-grid communities. Next, each topology was evaluated from a scale of 1 to 5 based on its performance in each criterion. It is important to note that the scores 1 to 5 denote lowest to highest scores gained by a topology for a specific criterion. For instance, [24] received a perfect score of (5/5) because it excelled in reducing the number of

components in the topology. Then the results were computed by multiplying the weights assigned to each criterion by the scores achieved by the topology on a scale of 5. After evaluating the existing topologies based on these criteria, an attempt was made to replicate the best-performing topology. This replication aimed to gain a deeper understanding of the topology and assess its feasibility in achieving similar results. Table 1 provides an overview of the comparisons among these topologies.

Criteria	Weights	[24]	[25]	[26]	[27]	[28]	[29]	[30]	[31]	[32]	[33]
Cost	**5**	(5/5)	(5/5)	(5/5)	(3/5)	(2/5)	(4/5)	(4/5)	(4/5)	(5/5)	(4/5)
Component count	**5**	(5/5)	(5/5)	(4/5)	(5/5)	(3/5)	(4/5)	(4/5)	(3/5)	(1/5)	(5/5)
Voltage Regulation	**4**	(4/5)	(4/5)	(3/5)	(4/5)	(4/5)	(4/5)	(3/5)	(3/5)	(3/5)	(3/5)
Power Efficiency	**3**	(5/5)	(4/5)	(4/5)	(5/5)	(5/5)	(4/5)	(4/5)	(3/5)	(4/5)	(3/5)
Control Methodology & Complexity	**2**	(3/5)	(3/5)	(3/5)	(3/5)	(3/5)	(3/5)	(2/5)	(2/5)	(2/5)	(3/5)
Results / Scores		87	84	75	77	62	74	68	60	58	72

Table 2.1: an overview of the comparisons between these topologies

Based on the aforementioned criteria, [24] stands out as the highest scorer, earning 87 out of 95 points. This achievement can be attributed to the authors' innovative approach of proposing a topology derivation method that minimizes the component count by effectively sharing components among separate converters. Consequently, this optimization resulted in a reduction of the overall cost and a substantial increase in power density for the design. Furthermore, the authors of [24] further validated their methodology by constructing a prototype that exhibited remarkable performance, surpassing other existing topologies in the evaluation. Their proposed TPC topology features only one inductor, three switches, and three diodes, as shown in Figure 2.4.

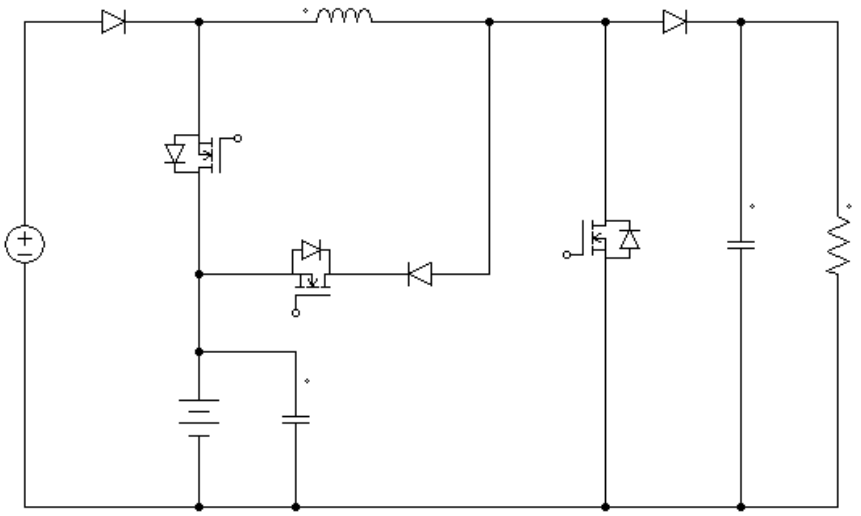

Figure 2.4: The proposed TPC topology in [24]

Chapter 3
Design of Three-Port Converter (TPC)

3.1 Topology Derivation Method

To achieve the objective of having two distinct output voltage levels, namely 12V and 48V, the battery voltage was set to one of the two voltage levels (i.e., 12V), and the DC link of the TPC was set to the other voltage level (i.e., 48V). A buck converter was incorporated between the PV panels and the battery to facilitate battery charging. Additionally, one boost converter was integrated between the PV panels and the DC bus, and another boost converter was integrated between the battery and the DC bus. These boost converters serve the purpose of elevating the voltage level to 48V to meet the requirements of the load. Figure 3.1 illustrates the TPC original circuit before the optimization of the topology.

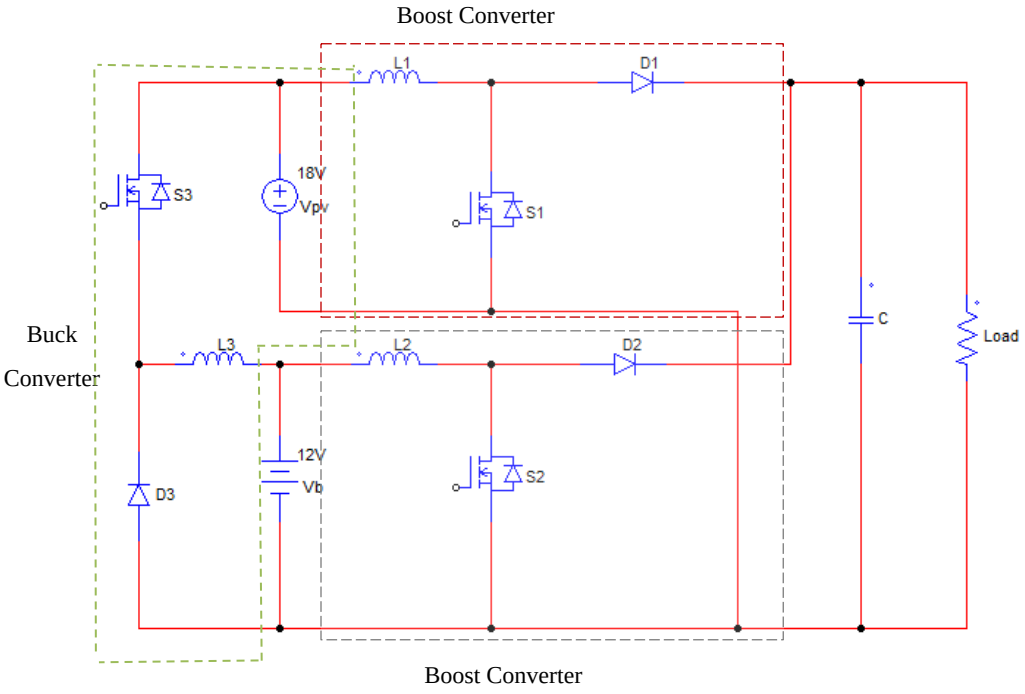

Figure 3.1: Original Circuit

3.1.1 Topology Optimization

In order to optimize the topology, the sharing of components among the different converters must be maximized. By doing so, one achieves cost-effectiveness and reduces the system complexity. To achieve component sharing, certain components, such as inductors, capacitors, and control circuitry, are used across all three converters wherever possible. In the following, the steps taken are described.

Step 1: Upon examining the topology, it became apparent that the L1-S1 and L2-S2 combinations shared an identical configuration. Therefore, these branches were merged to utilize a single shared inductor, as shown in Figure 3.2.

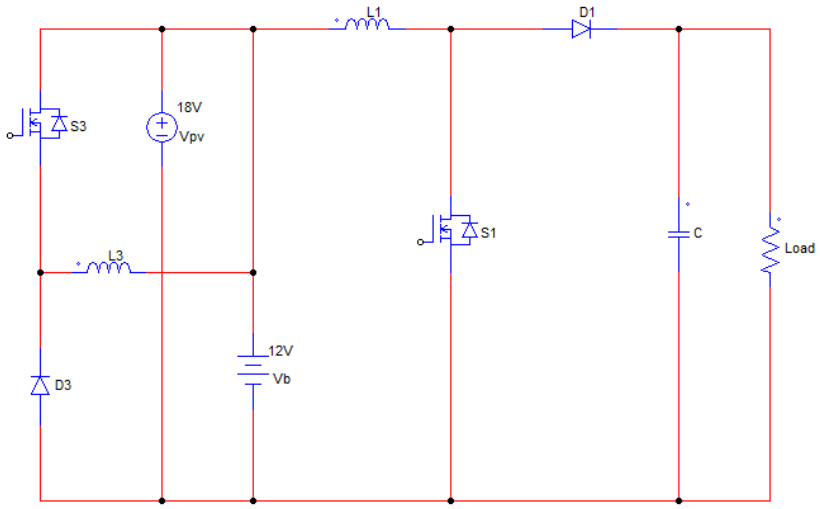

Figure 3.2: Step 1

Step 2: After merging the L1-S1 and L2-S2 branches, it became important to address the issue of an uncontrolled charging path that arose due to the voltage difference between the PV port (18V) and the battery port (12V). To prevent this undesired flow, a diode (D4) was introduced across the battery path, as shown in Figure 3.3. By incorporating a diode in this path, it was ensured that the current flowed from the battery to the load only in the desired direction.

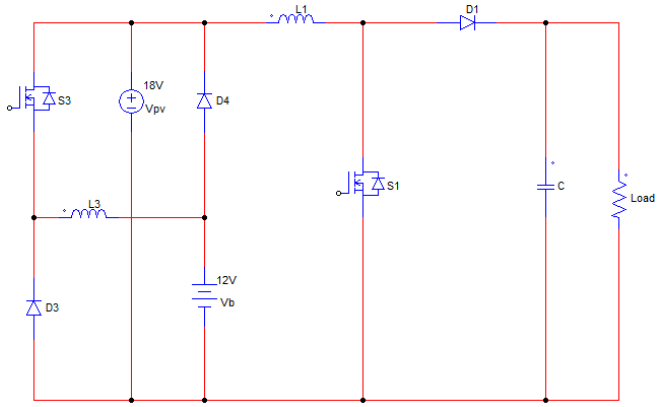

Figure 3.3: Step 2

Step 3: Upon further examination of the topology, it became evident that L1-S1 and S3-L3 combinations shared certain similarities when observed from the PV port. To optimize the system, the circuit was modified by moving the position of switch (S3) to the L1-S1 branch, allowing L1 to be shared, as shown in Figure 3.4.

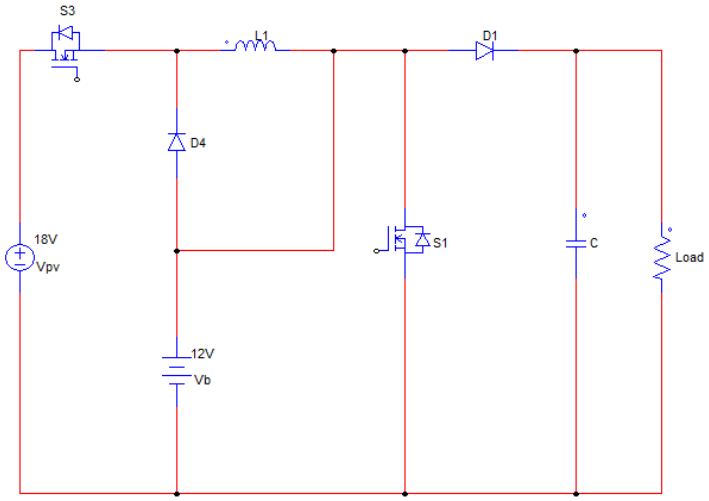

Figure 3.4: Step 3

Step 4: Following the adjustments made in step 3, it became apparent that the two power flows, one from the PV port to the load port and the other from the PV port to the battery port, could not be independently controlled without introducing a new switch (S4) in the battery path. Additionally, to prevent the battery from discharging through this path when the switch was open, a new diode (D5) was incorporated in series with the switch, as shown in Figure 3.5.

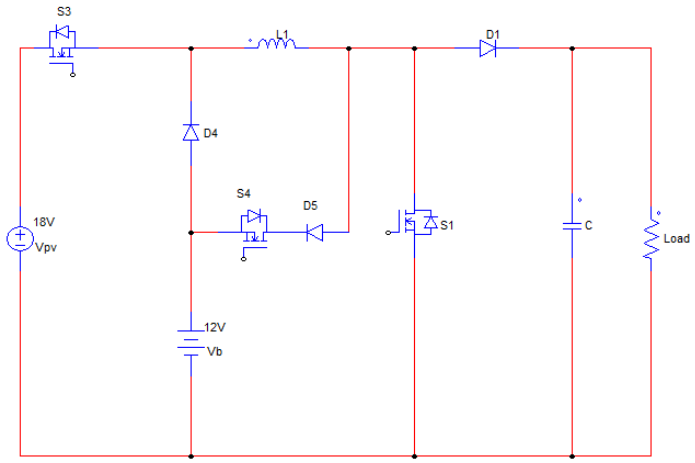

Figure 3.5: Step 4

Figure 5 depicts the final optimized topology, which utilizes only one shared inductor among the three converters. Based on the combination of Buck and Boost converter principles, this design will be referred to as Buck & Boost-TPC Topology. The specific operating conditions for this design are $V_{pv} > V_b$ (PV panel voltage higher than battery voltage), $V_{pv} < V_o$ (PV panel voltage lower than load voltage), and $V_b < V_o$ (battery voltage lower than load voltage).

3.2 Modes of Operation

To better analyze the proposed Buck & Boost TPC design, it was redrawn as shown in Figure 3.6. It is important to note that a large capacitor is used across the battery. The role of this capacitor is to filter the pulsating current that occurs during the charging and discharging processes of the battery.

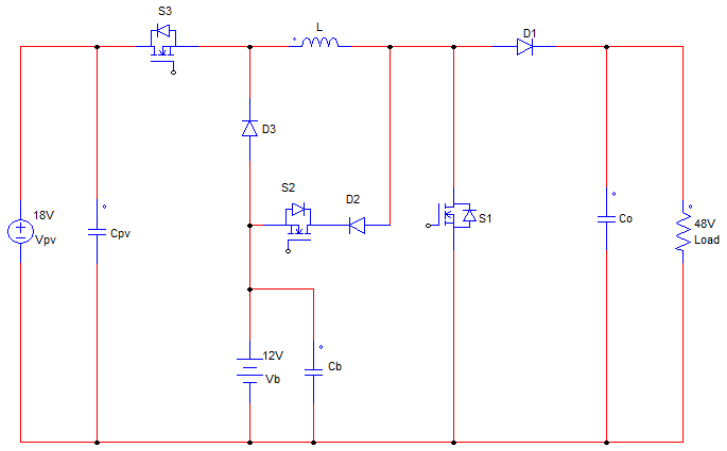

Figure 3.6: The proposed Buck & Boost TPC topology

TPCs typically operate in three different modes: Dual-Outputs (DO) mode, Dual-Input (DI) mode, and Single-Input Single-Output (SISO) mode. These modes are determined based on the specific requirements and characteristics of the system, including the availability of input sources, the power demand of the load, and the desired power flow control.

1) DO mode: This mode occurs when the power generated by the PV port exceeds the power demand of the load. Thus, the PV not only supplies power to the load but also charges the battery simultaneously. Figure 3.7 illustrates the equivalent circuit of the TPC in the DO mode.

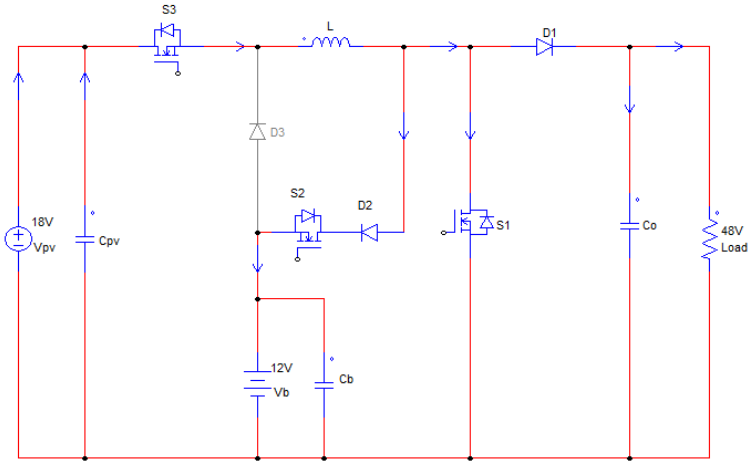

Figure 3.7: The Equivalent Circuit of the TPC in DO mode

In this mode, S3 is kept ON. There are three states within one switching period. The equivalent circuit for each state and the key waveforms are depicted in Figure 3.8 and 3.9, respectively. The gate signal voltage V_{GS} signals are the PWM signals, and duty ratios D1, D2, and D3 correspond to the ON times of switches S1, S2, and S3, respectively.

State I: S1 is turned ON, while S2 is turned OFF. The PV port only charges the inductor L (absorbing energy).

State II: S1 is turned OFF, while S2 is turned ON. The PV port continues to charge the inductor L (absorbing energy), and it also charges the battery.

State III: S1 is kept OFF, and S2 is turned OFF. The PV port and the inductor L (releasing energy) supply energy to the load.

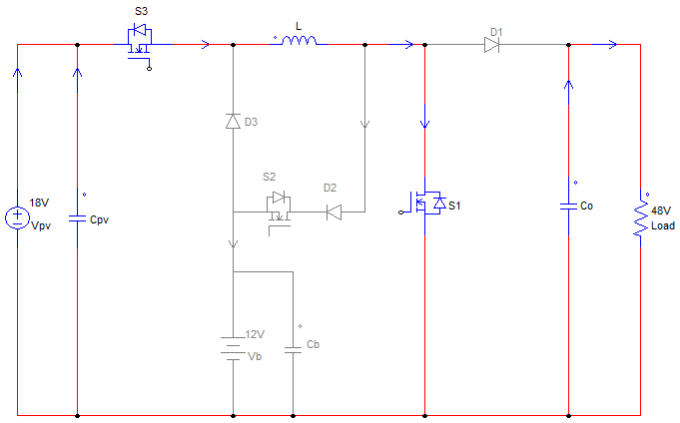

(a)

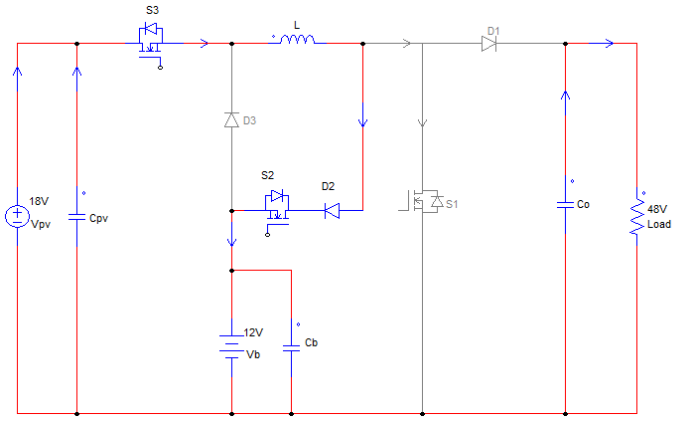

(b)

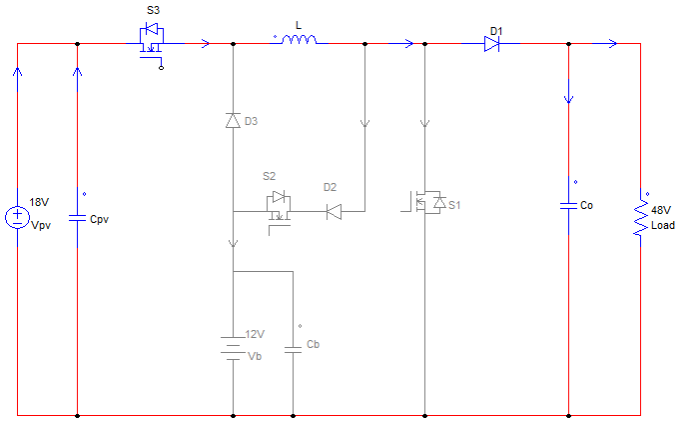

(c)

Figure 3.8: The equivalent circuits of each state in DO mode: (a) State I, (b) State II, and (c) State III

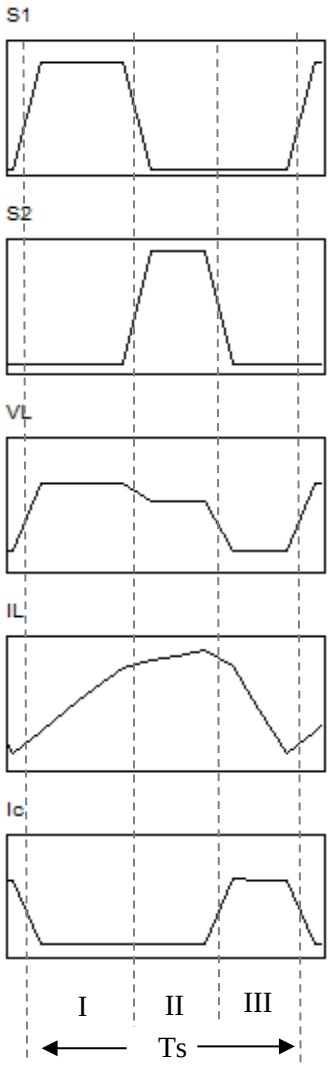

Figure 3.9: Key waveforms in DO mode corresponding to states I, II, and III

2) DI mode: this mode occurs when the power generated by the PV system is insufficient to meet the power demand of the load. Therefore, both the PV system and the battery work together to supply power to meet the load requirements. The equivalent circuit of the TPC in the DI mode is illustrated in Figure 3.10.

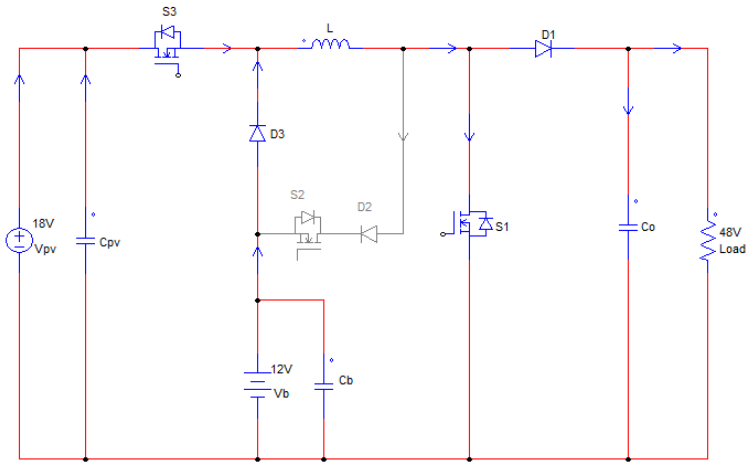

Figure 3.10: The Equivalent Circuit of the TPC in the DI mode

In this mode, S2 is kept OFF. There are four possible switching states in this mode. However, only three states are within one switching period. The equivalent circuit for each state is depicted in Figure 3.11. The key waveforms are shown in Figure 3.12 (a) for the three states I, II, and IV in one switching cycle when the duty cycle D1>D3. Figure 3.12 (b) shows the key waveforms for the three states I, III, and IV in one switching cycle when the duty ratio D3>D1.

State I: S1 and S2 are turned ON. The PV port only charges the inductor L (absorbing energy), while the output capacitor supplies the load.

State II: S1 is kept ON, while S3 is turned OFF. The battery port only charges the inductor L (absorbing energy), while the output capacitor supplies the load.

State III: S1 is turned OFF, while S3 is kept ON. The PV port and the inductor L (releasing energy) supply energy to the load and charge the output capacitor.

State IV: S1 is turned OFF, and S3 is kept OFF. The battery port and the inductor L (releasing energy) supply energy to the load and charge the output capacitor.

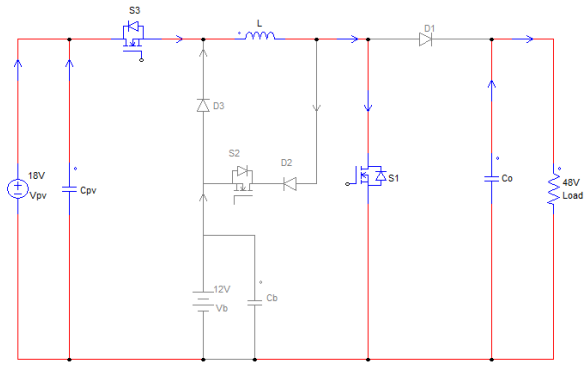
S3
L
D1
D3
S2
D2
S1
18V
Vpv
Cpv
Co
48V
Load
12V
Vb
Cb

(a)

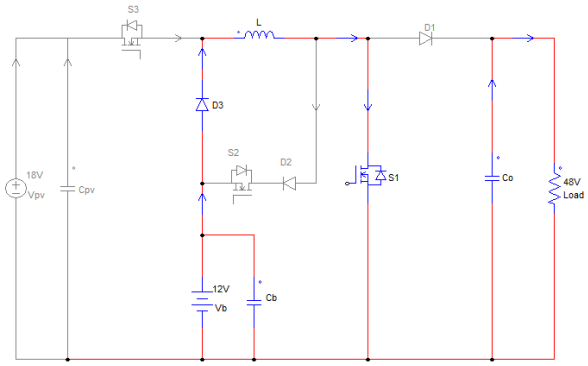
S3
L
D1
D3
S2
D2
S1
18V
Vpv
Cpv
Co
48V
Load
12V
Vb
Cb

(b)

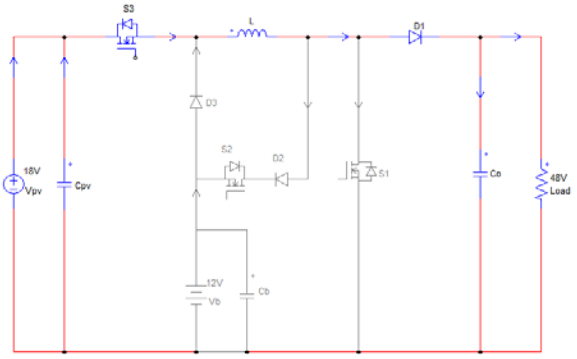
S3
L
D1
D3
S2
D2
S1
18V
Vpv
Cpv
Co
48V
Load
12V
Vb
Cb

(c)

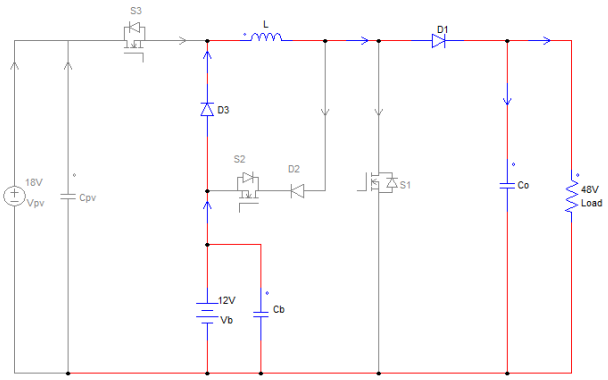

(d)

Figure 3.11: The equivalent circuits of each state in the DI mode: (a) State I, (b) State II, (c) State III, and (d) state IV

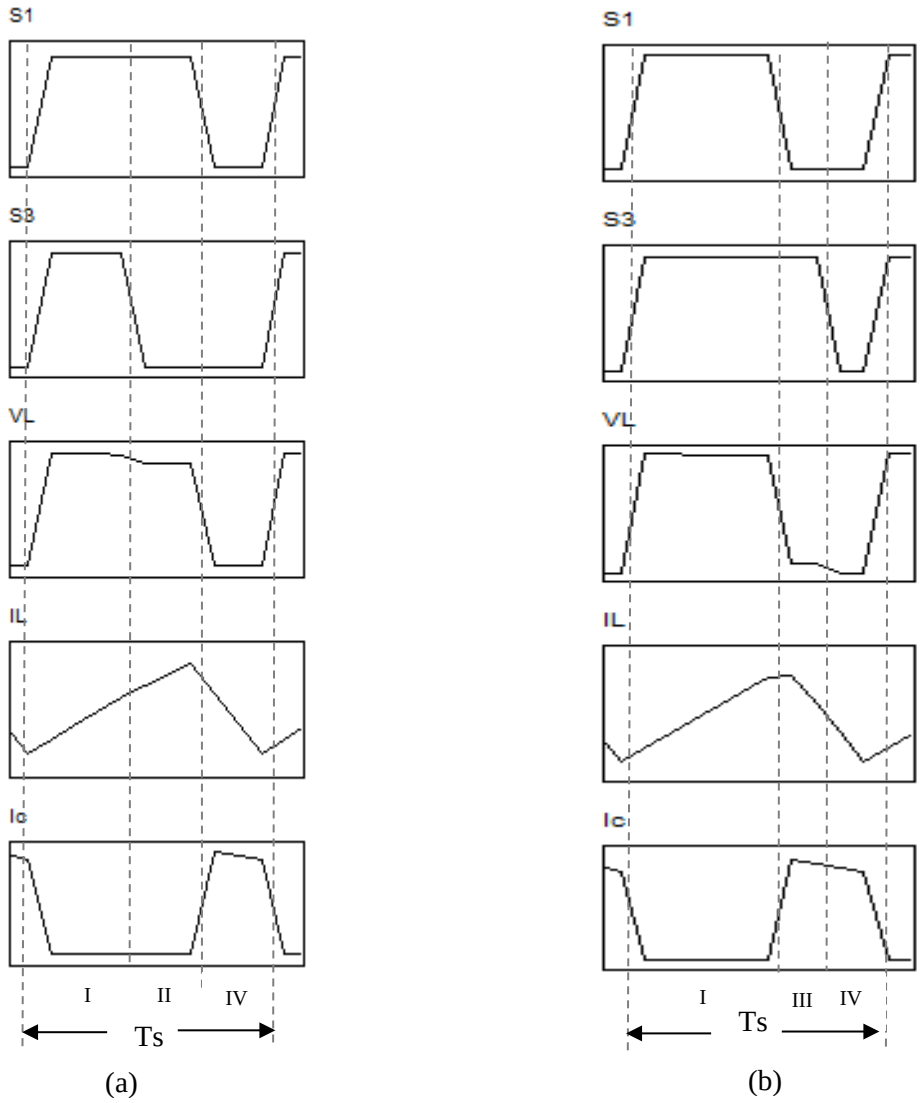

Figure 3.12: Key waveforms in DI mode corresponding to the states I, II, III, and IV: (a) D1 > D3 and (b) D1 < D3.

3) SISO mode: in this mode, the TPC will operate as either a conventional buck or a conventional boost converter. This can happen in three scenarios.

Scenario (a): In the absence of power generation from the PV system, the load is solely powered by the battery. In this case, the TPC functions as a conventional boost converter. Figure 3.13 (a) depicts the equivalent circuit in this specific scenario.

Scenario (b): When the battery reaches its full charge, the PV system will solely supply power to the load. In this case, the TPC will operate as a conventional boost converter. Figure 3.13 (b) illustrates the equivalent circuit in this scenario.

Scenario (c): If no load is connected at the output terminals, the PV system will solely focus on charging the battery. Figure 3.13 (c) represents the equivalent circuit in this particular situation.

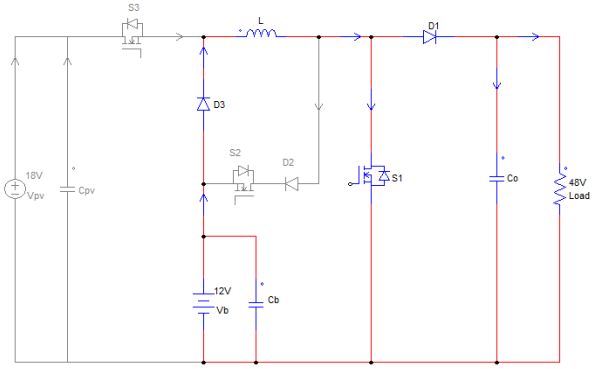

(a)

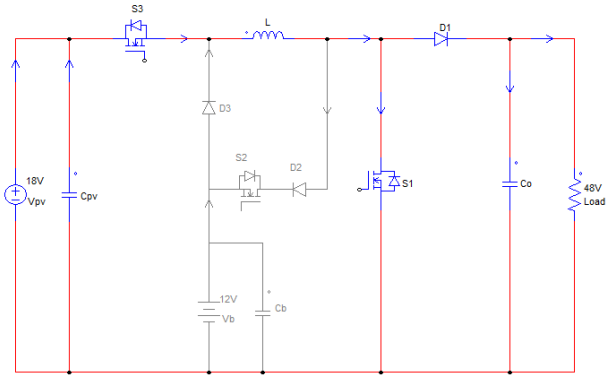

(b)

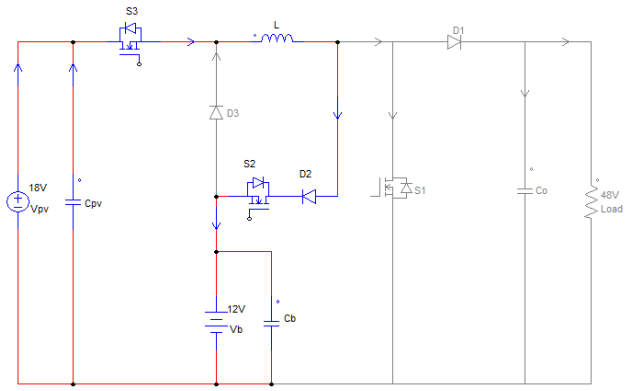

(c)

Figure 3.13: The Equivalent Circuits of the TPC in the SISO mode for scenarios (a), (b), and (c)

3.3 System Specifications

To size the system, a load profile specific to an individual household in Zimbabwe was chosen from the existing literature. To simplify the design process, this load profile was scaled down by a factor of 7. Additionally, an insolation profile representing the solar radiation for the same location was obtained from the internet. The primary objective was to meet the load requirements on an instantaneous basis, while also adhering to the limitations of the renewable energy source, energy storage system, and other system components. Moreover, the system must fulfill the requirements expected by the load in terms of stability and reliability.

3.3.1 Load Profile

Figure 3.14 displays a load profile for an individual household in Zimbabwe [37] that has been scaled down by a factor of 7. This scaling was done in order to compare the results of the proposed topology to other topologies in the literature. The load profile indicates the power demand of the household over 24 hours. The total energy demand per day is reported to be 1.1 kWh. The highest power demand recorded in the profile is 97.14 W, while the lowest power demand is 25.71 W.

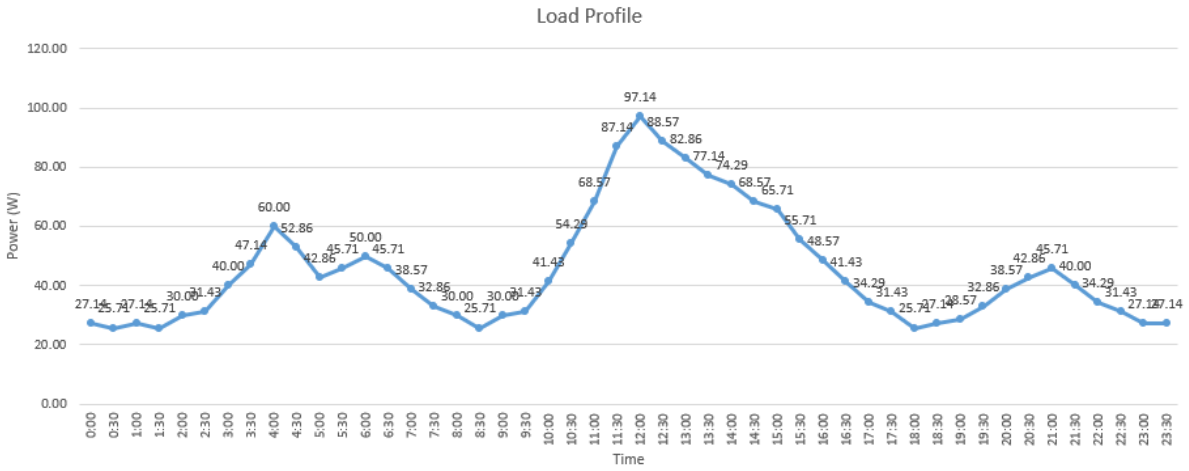

Figure 3.14: The load profile of an individual household in Zimbabwe [35] scaled down by a factor of 7

3.3.2 Insolation Profile

Figure 3.15 illustrates the solar insolation profile for a typical day in Zimbabwe [38]. The peak solar radiation point recorded in this profile is 776.92 kW/m^2, representing the highest intensity of solar energy received during that day.

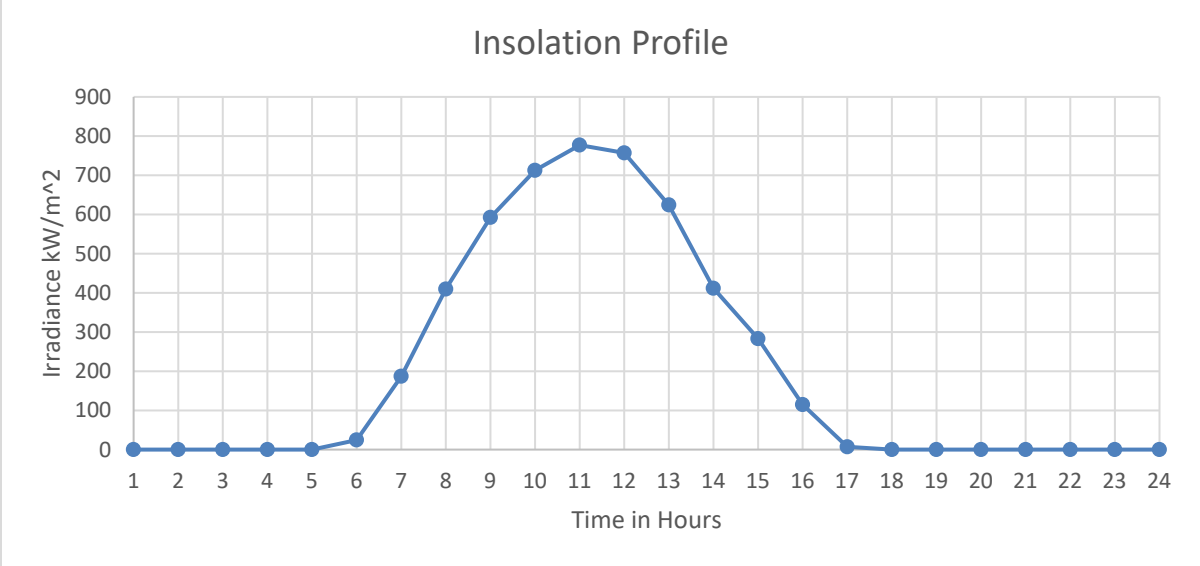

Figure 3.15: The insolation profile for June 1, 2021 in Zimbabwe [38]

3.3.3 Battery Bank Sizing

Based on the solar insolation level and the load profile, it is possible to calculate the energy generated and absorbed in 24 hours. The load profile indicates a total energy demand of 1.1 kWh per day. This value represents the cumulative energy required by the household during a 24-hour period. Equation (1) provides a practical method for sizing the battery system, taking into account several factors including the daily energy consumption, desired days of autonomy, battery state of charge (SoC), and efficiency.

$$Battery\ Capacity = \frac{Daily\ Energy\ Use\ \times\ Days\ of\ \ Autonomy}{(1-SoC)\times\ Efficiency} \tag{1}$$

where

- Daily Energy Use refers to the total energy consumed by the load in a single day.
- Days of Autonomy represents the desired number of consecutive days the battery can support the load without recharging.
- SoC denotes the desired state of charge at the end of the autonomy period.
- Efficiency signifies the overall efficiency of the battery system, considering factors like charging and discharging losses.

By applying Equation (1), one can determine the battery capacity necessary to meet the specified energy requirements, autonomy period, SoC, and efficiency considerations.

3.3.4 TPC Specifications

The inductor value has been selected based on the specification given in Table 1. When selecting the inductor value, it was essential to consider all the power paths within the system, including the PV-Load path, Battery-Load path, and PV-Battery path. Each of these paths plays a role in supplying power to the load and managing energy flow within the system. Furthermore, to ensure the inductor value was chosen correctly, we investigated all potential load variations. This investigation helped ensure that the inductor can effectively handle varying load requirements while meeting the load's power demands. Appendix A explains the process of selecting the appropriate value for the inductor and the capacitor.

PV Voltage (open circuit voltage at isolation level of 1 kW/m^2)	18V
Battery Voltage (open circuit voltage at soc=1)	12V
Output Voltage (load terminals)	48V
Load Variation Range	25W -100W
Switching Frequency	100kHz
Inductor Current Ripple Limit	20%
Inductor Size	200uH

Table 3.1: TPC Specifications and Inductor Size

3.4 Control Unit

The power flow and modes of operation of the TPC are determined by the available solar power, the load demand, and the battery SoC. To regulate the output load voltage and the battery current, a nested Proportional-Integral (PI) control loop was employed. It was important to regulate the battery current during both charging and discharging to prevent exceeding the battery's limitations and ensure its proper operation. For the PV port, the Maximum Power Point Tracking (MPPT) technique was employed to ensure optimal power extraction from the solar panels. The Perturb and Observe (P&O) algorithm is commonly used to achieve MPPT. This algorithm continuously adjusts the operating point of the PV system to track the maximum power point, ensuring maximum power generation from the available solar resource. Figure 3.16 depicts the control diagram for the TPC.

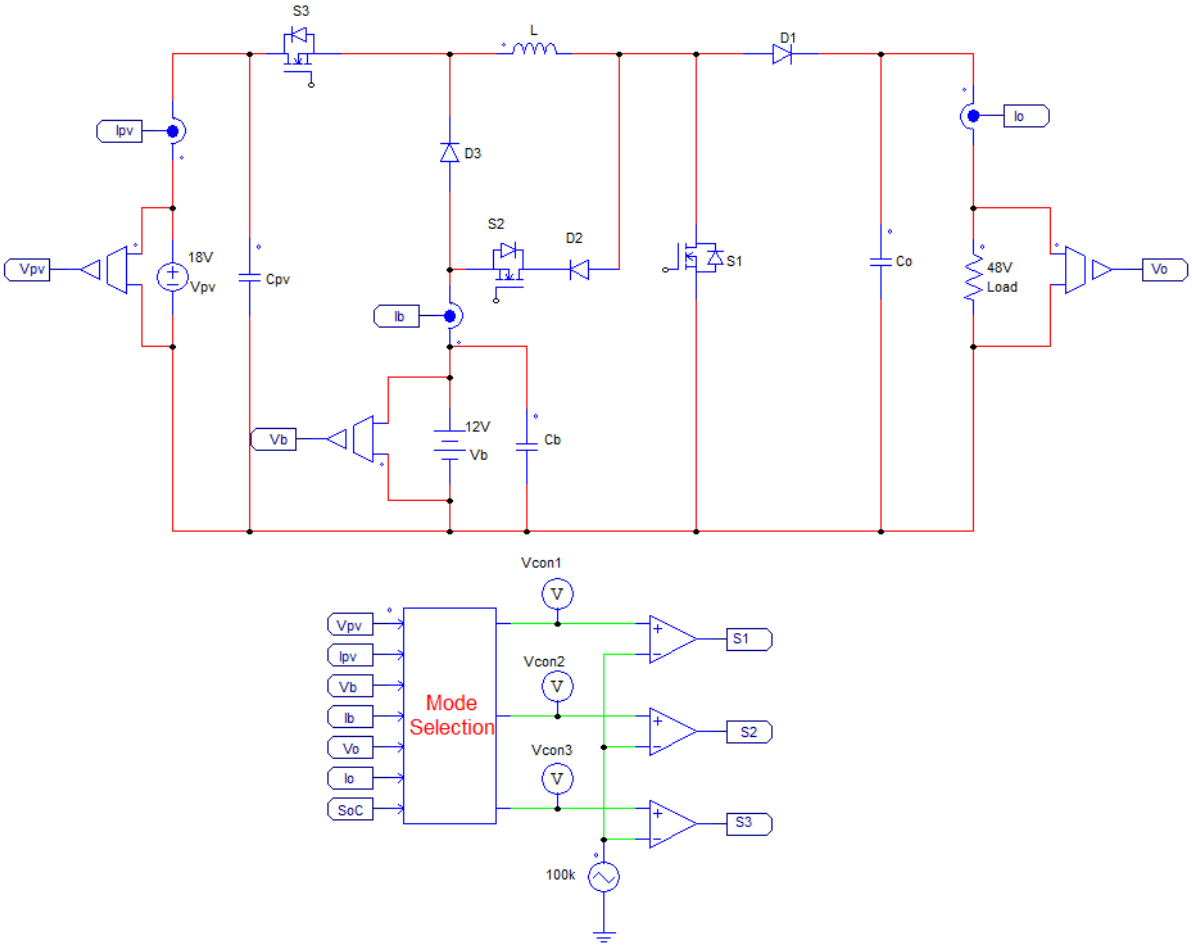

Figure 3.16: Control diagram for the TPC

The mode selection flow chart, shown in Figure 3.17, outlines the decision-making process within the system. It determines the appropriate mode of operation based on the prevailing conditions, such as solar power availability, load demand, and battery SoC. By following this flow chart, the TPC can dynamically adapt to the conditions and switch between different modes to optimize power flow and meet the system's requirements. The controlling method and the mode selection flow chart is translated into C-code. Appendix B shows the C-code used in the simulation.

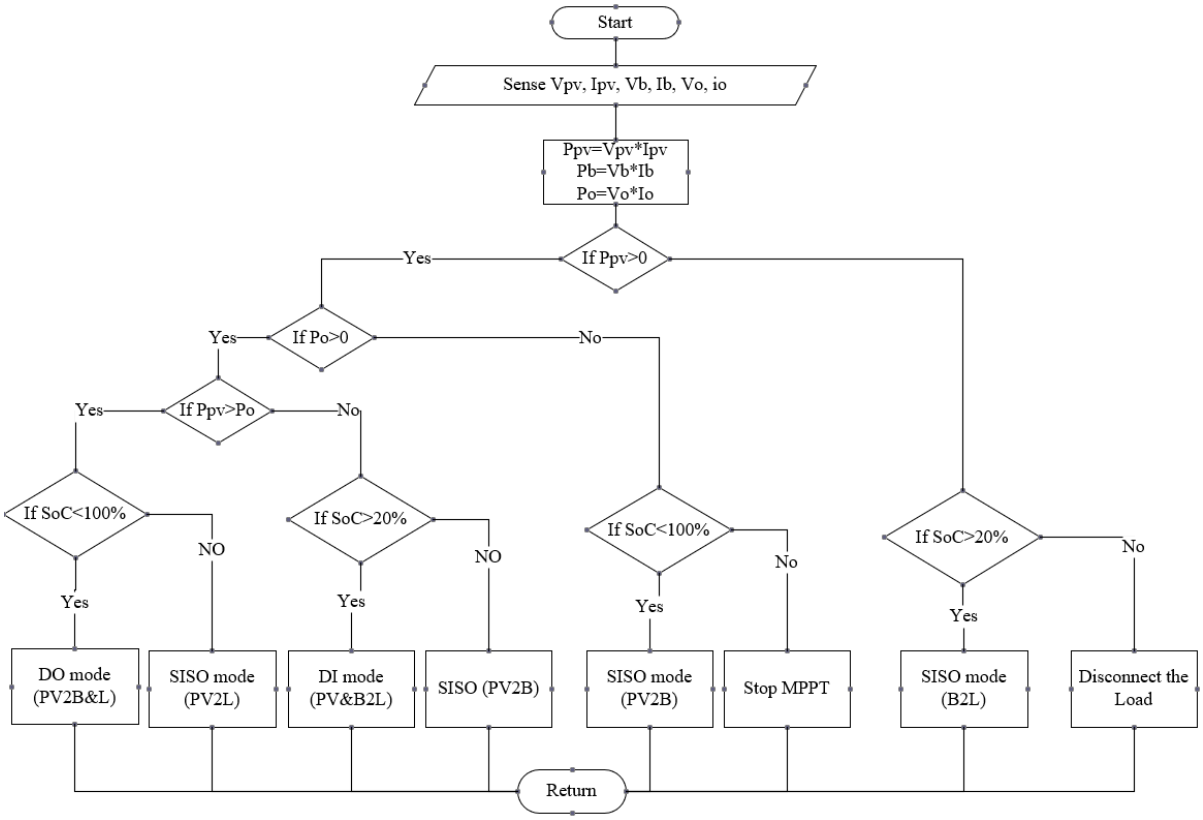

Figure 3.17: Mode selection flow chart

1) DO mode (PV2B&L):
    - S1 is regulating the output voltage.
    - S2 is achieving MPPT.
    - S3 is always ON.
2) DI mode (PV&B2L):
    - S1 is regulating the output voltage.
    - S2 is always OFF.
    - S3 is achieving MPPT.
3) SISO mode:

a. PV2L:

- S1 is regulating the output voltage.
- S2 is always OFF.
- S3 is always ON.

b. B2L:

- S1 is regulating the output voltage.
- S2 is always OFF.
- S3 is always OFF.

c. PV2B:

- S1 is always OFF.
- S2 is always ON.
- S3 is achieving the MPPT.

The simulation and results for different modes are provided and discussed in Chapter 4.

Chapter 4
Simulation Results and Discussions

To assess the performance of the proposed topology, a comprehensive simulation analysis was conducted using PSIM software [39]. To emulate a PV source, a solar module (Physical model) from the PSIM library was used. Additionally, to simulate a load profile over a 24-hour period, a piecewise current source was employed at the DC Bus. Moreover, a lithium-ion battery model, as described in [40], was integrated into the simulation. This model allows for the observation of essential battery characteristics, such as State of Charge (SoC), charging and discharging current waveforms, open-circuit voltage, etc. Furthermore, to accurately measure losses and evaluate the overall efficiency of the design, thermal modules for MOSFETs and diodes in PSIM were incorporated. The specifications for these modules were derived from the datasheets of the respective devices, ensuring a realistic representation of their thermal behavior during the simulation.

4.1 Modes of operation

To evaluate the functionality of the proposed topology (see Figure 3.6), comprehensive testing was conducted under various scenarios that may occur during both day and night. The steady-state waveforms, such as output voltage, PV power, output power, and battery current, are presented for all operational modes.

1) DO mode:

   In this mode, the power generated by the PV port exceeds the power demand of the load. Therefore, the surplus power charges the battery. Figure 4.1 shows that the voltage is maintained at 48V during this mode. Additionally, the battery current is negative, indicating that the battery is being charged.

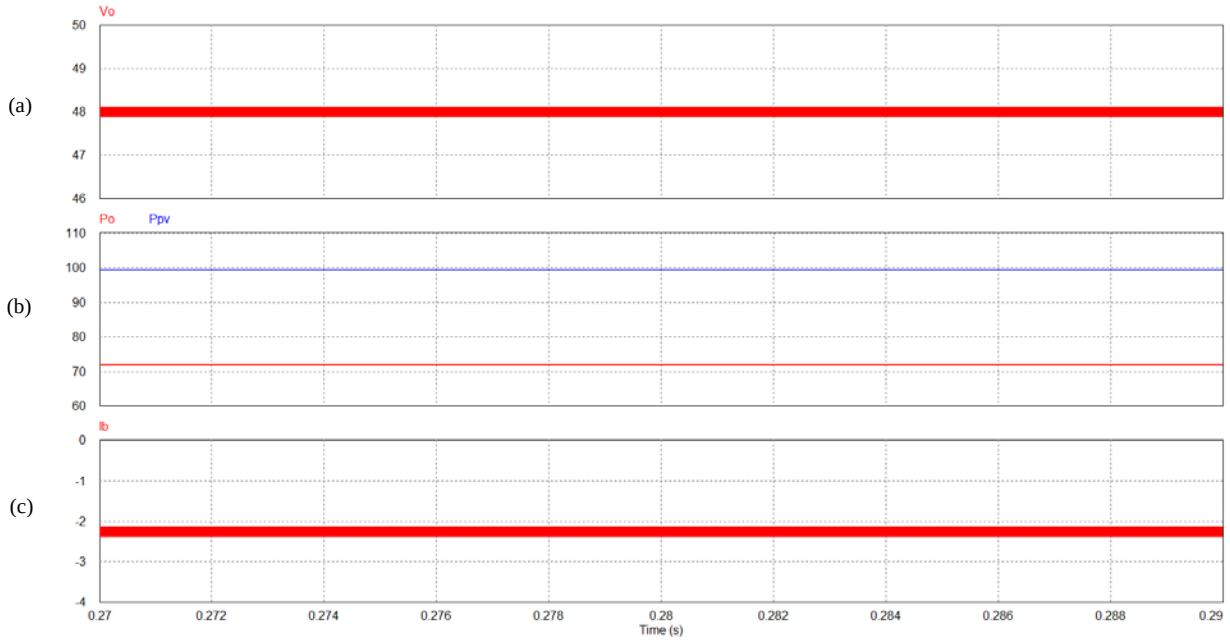

Figure 4.1: Steady-state waveforms in DO mode: (a) Output voltage, (b) output and PV power, and (c) battery current

2) DI mode:

In this mode, the power generated by the PV system is insufficient to meet the power demand of the load. Therefore, the deficit power will be drawn from the battery to supply the load. Figure 4.2 shows that the voltage is regulated at 48V throughout this mode. Additionally, the battery current is positive, indicating that the battery is being discharged.

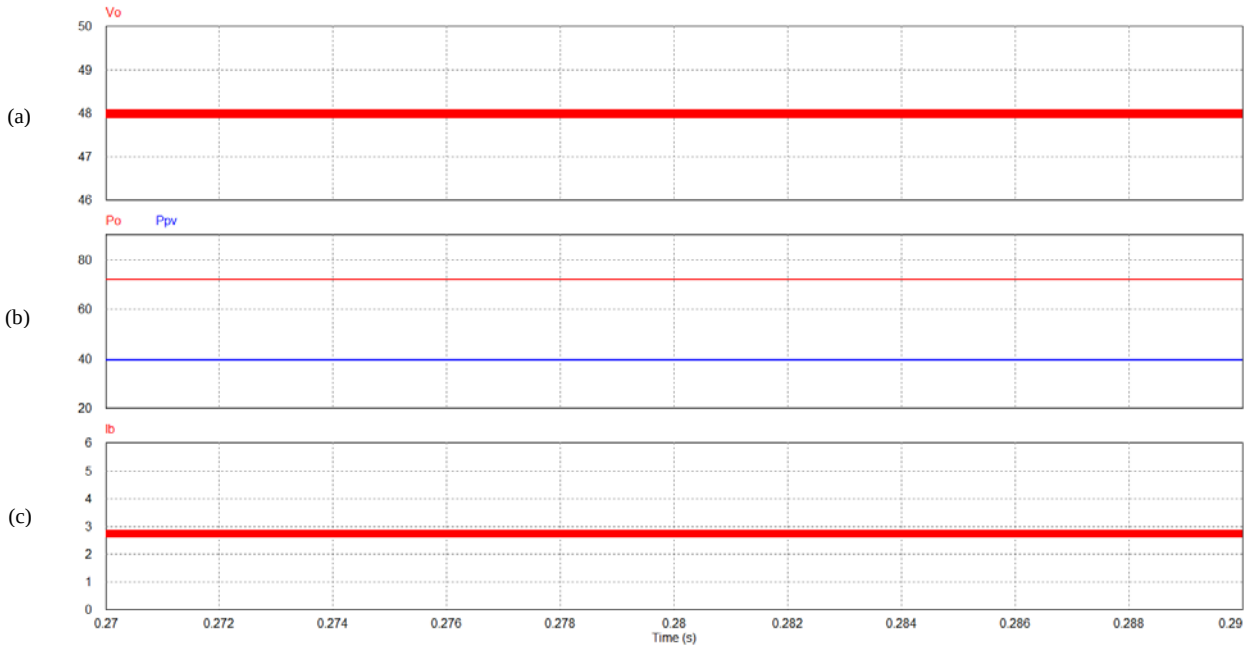

Figure 4.2: Steady-state waveforms in DI mode: (a) Output voltage, (b) output and PV power, and (c) battery current

3) SISO mode:

This mode has three scenarios:

a. In the absence of power generation from the PV system, the load is solely powered by the battery (B2L). Figure 4.3 (a) shows that the voltage is regulated at 48V while the battery solely supplies the load.

b. If the battery is fully charged and available PV power is higher the load, the PV will solely supply power to the load (PV2L). In this case, MPPT is not used. Figure 4.3 (b) shows that the voltage is regulated at 48V while the PV power is equal to the load demand.

c. If no load is connected at the output terminals, the PV system will solely focus on charging the battery (PV2B), as shown in Figure 4.3 (c).

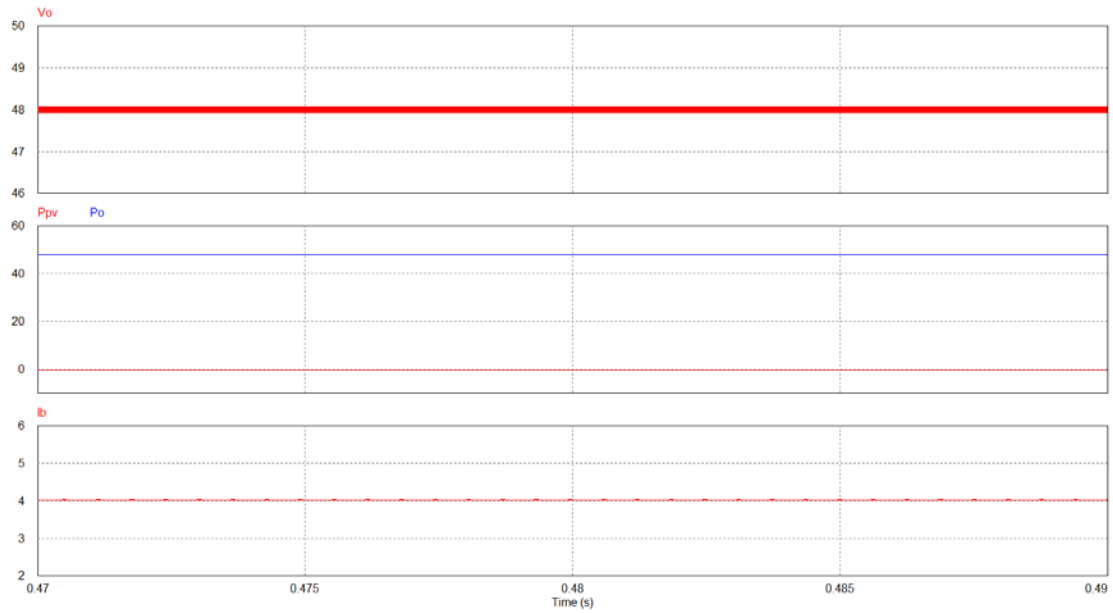
Vo
50
49
48
47
46
Ppv
Po
60
40
20
0
Ib
6
5
4
3
2
0.47
0.475
0.48
0.485
0.49
Time (s)

(a)

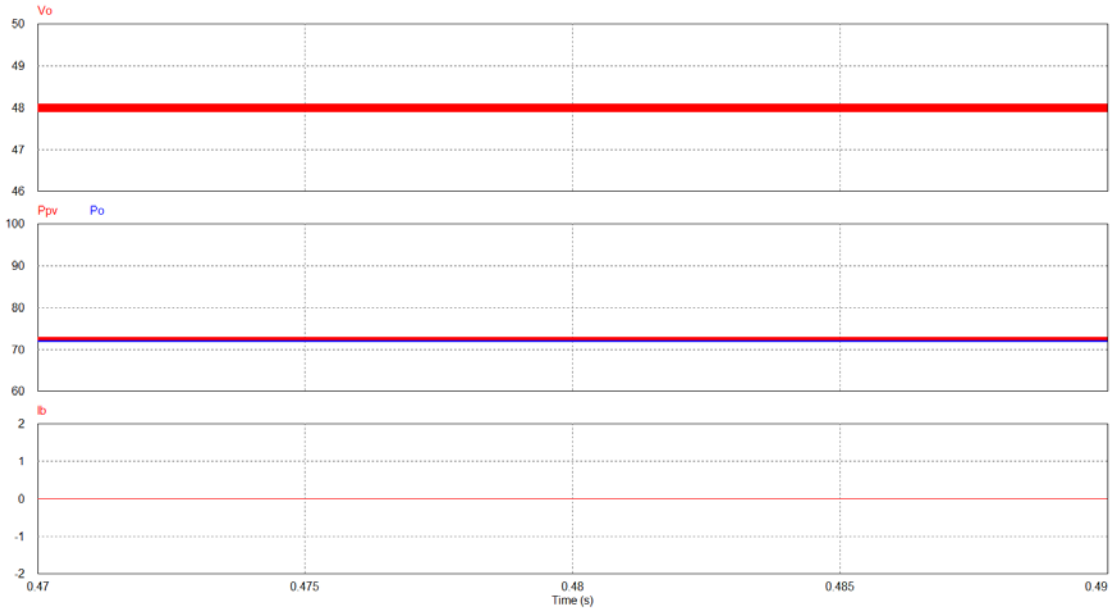
Vo
50
49
48
47
46
Ppv
Po
100
90
80
70
60
Ib
2
1
0
-1
-2
0.47
0.475
0.48
0.485
0.49
Time (s)

(b)

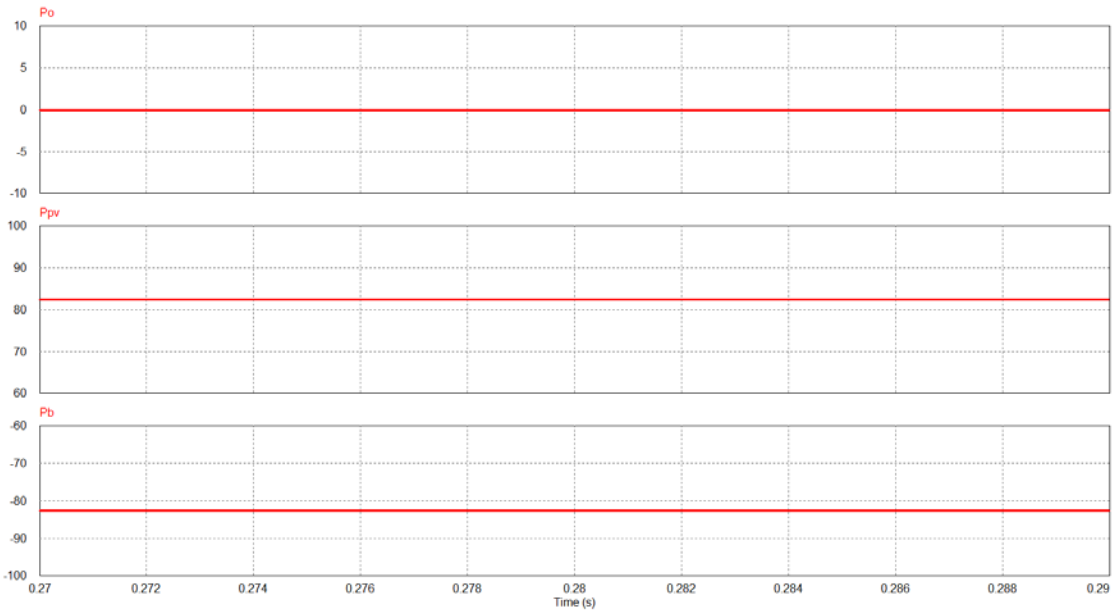

(c)

Figure 4.3: Steady-state waveforms in SISO mode: (a) B2L, (b) PV2L, and (c) PV2B

4.2 Transition between modes of operation

Another important aspect to evaluate in the proposed topology is mode transition during operation. Figure 4.4 illustrates the sequence of transitions between modes. The sequence begins with the SISO mode which occurs at night time when there is no PV power, and the battery supplies all the load. This mode is followed by the DI mode which mostly happens at the beginning of the day when PV power is insufficient to meet the load demand. Therefore, the battery supplies the deficit power required by the load. Subsequently, the DO mode occurs during the middle of the day when PV power reaches its peak. The load demand is fully supplied by the PV power, and any surplus power is used to charge the battery.

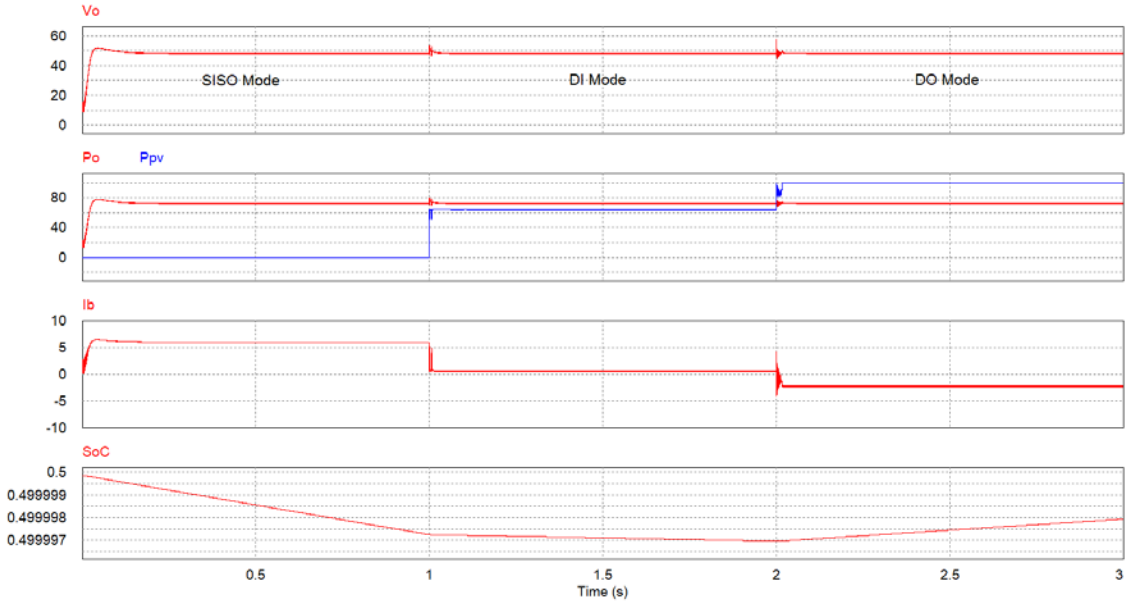

Figure 4.4: Waveforms of transition between modes of operation

4.3 Power Efficiency

To measure the losses of the design, PSIM software provides thermal modules for MOSFETs and diodes. Different modes with different range of loads were tested to calculate the efficiency of the design. Figure 4.5 shows the efficiency curves for the proposed design.

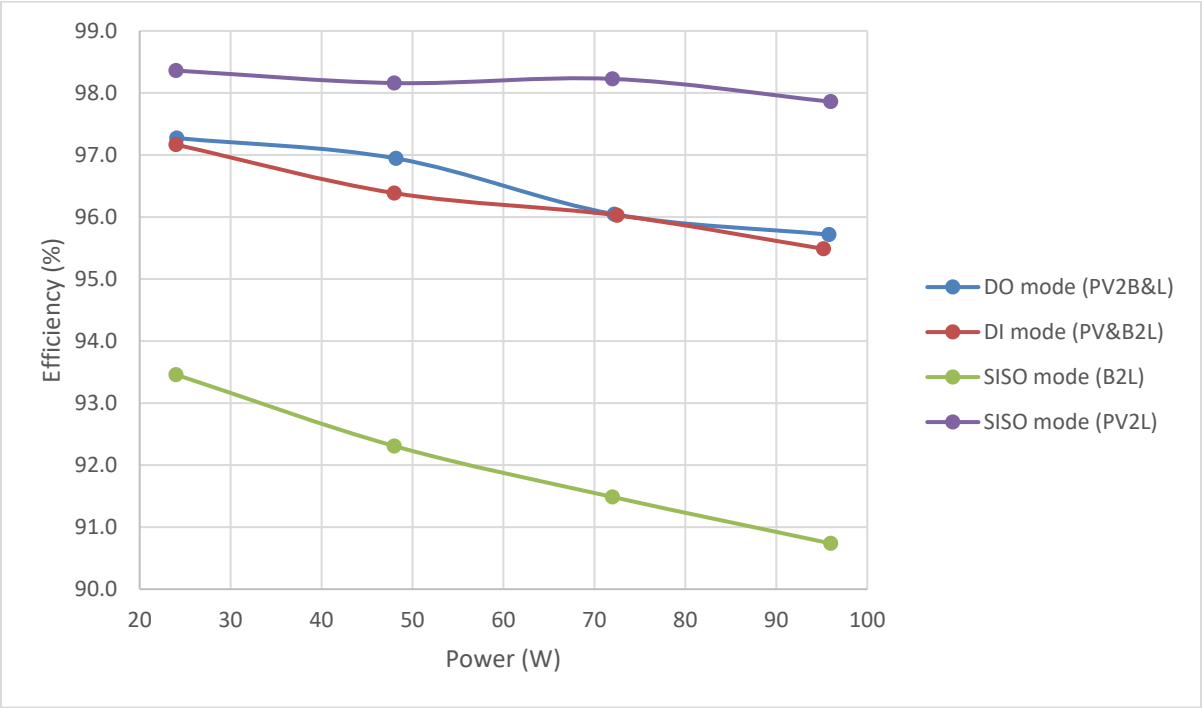

Figure 4.5: Efficiency curves for the proposed design

It is important to highlight that the SISO mode (B2L) exhibits relatively lower efficiencies when compared to other modes because of the deliberate setting of the battery voltage to 12V. This mode only occurs during nighttime periods. In this period, most of the loads are light, and they are directly connected to the 12V battery. Therefore, the 48V DC bus is not needed for this period of time. However, in scenarios where a customer prioritizes the 48V port during nighttime operations, a viable solution would be adjusting the battery voltage to 24V or higher. This modification serves the purpose of reducing battery current, thereby lowering losses. A simulation test was done for the proposed design when using a 24V battery instead of a 12V battery, and the efficiency at full load (100W) was enhanced from 90.7% to 95.8% as shown in Figure 4.6.

Figure 4.6: Efficiency comparison of SISO mode (B2L) for 12V and 24V battery

The comparison between the proposed topology and other topologies is given in Table 4.1. The proposed topology features one single inductor, three switches, and three diodes. Utilizing only one single inductor instead of two single inductors or a coupled inductor reduces the cost and size and thus enhances power density. Also, to achieve all the aforementioned modes of operation, each topology should at least have three controllable switches. Number of diodes differs for different topologies depending on the requirement of the circuit. Most topologies use three diodes to control the current path within the circuit.

Topology	Type	Rated Output Power (W)	PV Voltage (V)	Battery Voltage (V)	Output Voltage (V)	Switching Frequency (kHz)	Component Count				Average Efficiency (%)
							Switches	Diodes	Inductors		
									Single	Coupled	
[24]	Highly Integrated Configuration	500	35-70	60-80	100	100	3	3	1	-	97.2
[25]		35	20-30	12	5	20	3	3	1	-	88
[26]		200	24	36	380	30	2	3	1	1	94.8
[27]		80	18	12	48	50	3	1	-	1	93.7
[28]		200	40	48	100	100	4	5	-	1	95.1
[29]		200	18	12	24	20	4	4	3	-	93.6
[31]		350	15	10	293	40	6	2	4	-	86
[32]		150	72	36	-	50	4	5	-	2	95.6
[33]		250	17	36	50	15	4	3	2	-	-
Proposed TPC		100	15-18	12	48	100	3	3	1	-	95
Conventional TPC	Traditional Configuration	100	15-18	12	48	100	3	1	2	-	97.1

Table 4.1: comparison between the proposed topology and other topologies

Several factors can impact efficiency, including power range, voltage levels of ports, active components in the path of low voltage ports, etc. For instance, in [24], port voltage levels are 60V for PV, 80V for battery, and 100V for output. This voltage selection reduces transferred current between ports, leading to reduced losses. Moreover, while the literature suggests that highly integrated TPCs generally achieve superior efficiency compared to traditional ones with multiple conversion stages, this argument is not always right. Highly integrated TPCs use more diodes than traditional TPCs to direct the currents within the circuit. These diodes have conduction losses which add to the total losses and reduce the efficiency of the converter. A replication for the proposed TPC in [24] was conducted in PSIM to gain a deeper understanding of the highly integrated TPCs and to compare them with the traditional TPC shown in Figure 2.3. The simulation showed that the traditional TPC had a higher efficiency than the highly integrated TPC that was proposed. The average efficiency for the traditional TPC was 98.4%, while the proposed TPC attained an efficiency of 97.2%.

It's worth mentioning that traditional TPCs exhibit slightly higher efficiencies when compared to the highly integrated TPCs. This disparity can be attributed to the additional diodes integrated into the highly integrated TPCs. However, it's important to note that traditional TPCs utilize two inductors, which leads to increased design cost and size.

The dual output voltage feature stands out as a noteworthy feature offered by the proposed converter, distinguishing it from other highly integrated TPC topologies found in existing literature. While all TPC topologies can be classified as dual output configurations, only the proposed design incorporates the unique feature of combining a battery port with a lower voltage than the PV port and an output port with a higher voltage than the PV port. This feature empowers individuals in off-grid communities by providing them with a versatile solution. It offers a 12V output port for powering low-power electrical appliances, catering to the majority of their everyday needs, while also offering a 48V output for high-power electrical appliances, thereby expanding their range of usable devices and enhancing overall utility.

4.4 Case Study I: Load Profile for Zimbabwe

To further evaluate the functionality of the proposed design, a case study was conducted for Zimbabwe over a 24-hour period using PSIM. The study involved obtaining a solar insolation profile for a typical day in Zimbabwe from the NASA Prediction of Worldwide Energy Resources database. The system was then appropriately sized to meet the load requirements. Figure 4.7 illustrates the proposed TPC.

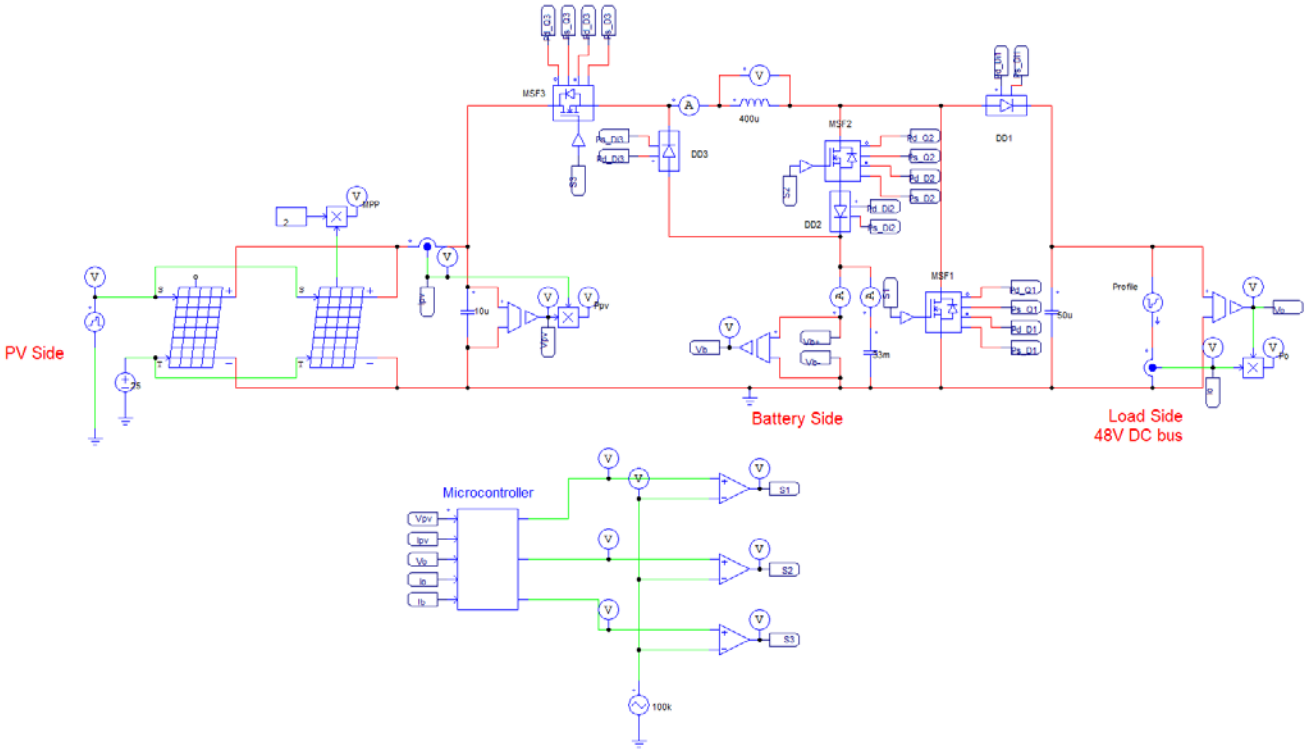

Figure 4.7: The proposed TPC with a load profile at 48V DC bus

The primary objectives of this case study are as follows:

- Observe and analyze the system's response to different scenarios during the 24-hour period.
- Ensure that the DC bus voltage is regulated effectively during all modes of operation.
- Verify that the converter efficiently tracks the Maximum Power Point (MPP) whenever there is sunlight available, and the PV power does not exceed the power demand of the load plus the permitted charging current power of the battery.

In order to expedite the running time of the simulation in PSIM, the 24-hour duration is scaled down to 24 seconds. This scaling allows for faster simulation and analysis of the system's performance over the entire day.

Figure 4.8 shows the DC bus voltage (V_o), load profile (P_o), and solar insolation profile (irradiance) from PSIM simulation for Zimbabwe. It can be seen that throughout the 24-hour period, the output voltage is consistently regulated, adapting to changes in the load profile according to the varying demand. Simultaneously, the irradiance profile dynamically adjusts in response to the availability of sunlight.

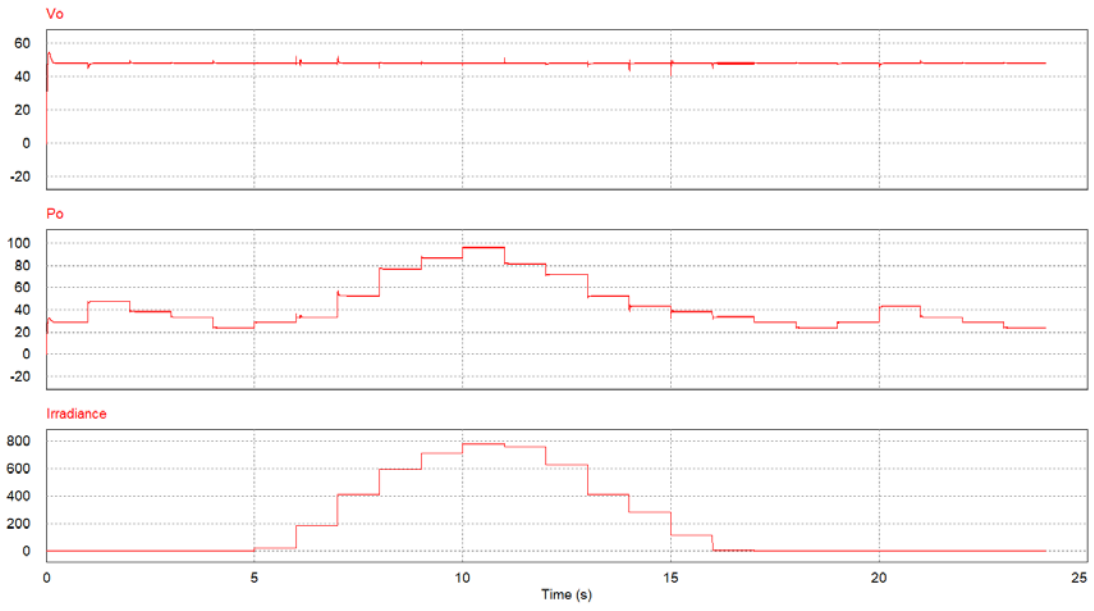

Figure 4.8: DC bus voltage (V_o), load profile (P_o), and solar insolation profile (irradiance) from PSIM simulation for Zimbabwe

Figure 4.9 depicts the DC bus voltage (V_o), the PV and load Power (P_{pv} & P_o), and the battery currents (I_b) from PSIM simulation. Battery is charging or discharging based on the power generated by the PV source and the power consumed by load. Negative battery current refers to charging state, whereas positive battery current refers to discharging state. It can be seen from the figure that when the power generated by the PV source is higher than the power consumed by the load, the battery is charging. In contrast, when the power generated by the PV source is lower than the power consumed by the load, the battery is discharging.

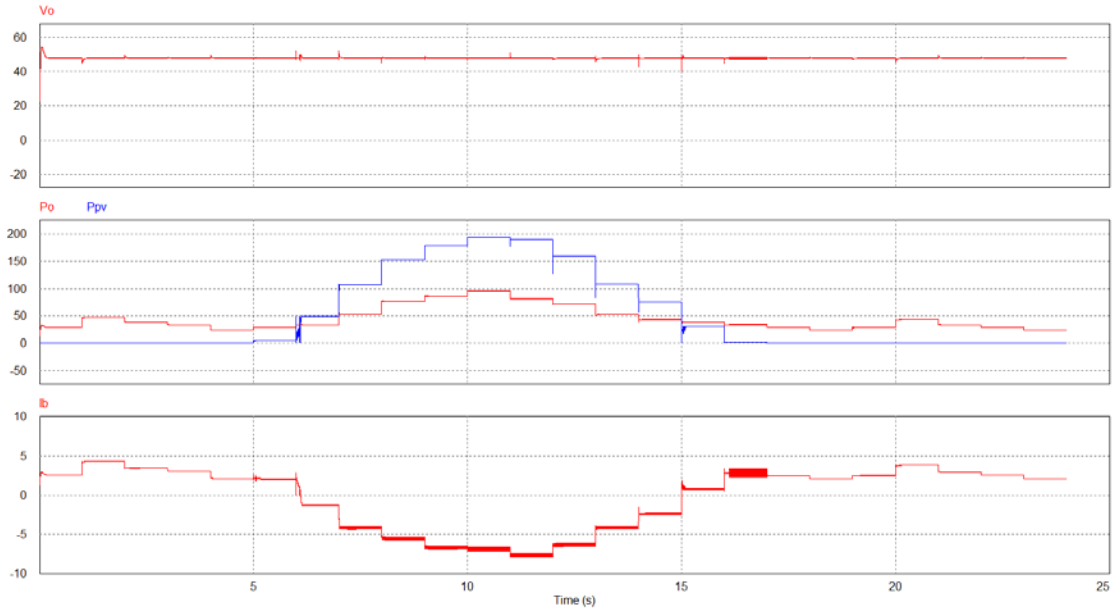

Figure 4.9: The DC bus voltage (V_o), the PV power and load profile (P_{pv} & P_o), and the battery current from PSIM simulation for Zimbabwe

Figure 4.10 displays the DC bus voltage (V_o), the exact Maximum Power available, and the measured PV power (P_{pv}) obtained from the PSIM simulation. In this figure, the Maximum Power point (MPP) waveform depicts the accurate maximum power point tracking values based on the calculated results of the solar panel modules, while the P_{pv} waveform represents the measured results from the 24-hour profile simulation. It is evident that the controller is effectively tracking the MPP as shown in (P_{pv}) waveform while regulating the DC bus voltage. It is significant to track the MPP to extract the maximum power from the solar panel modules whenever there is sunlight.

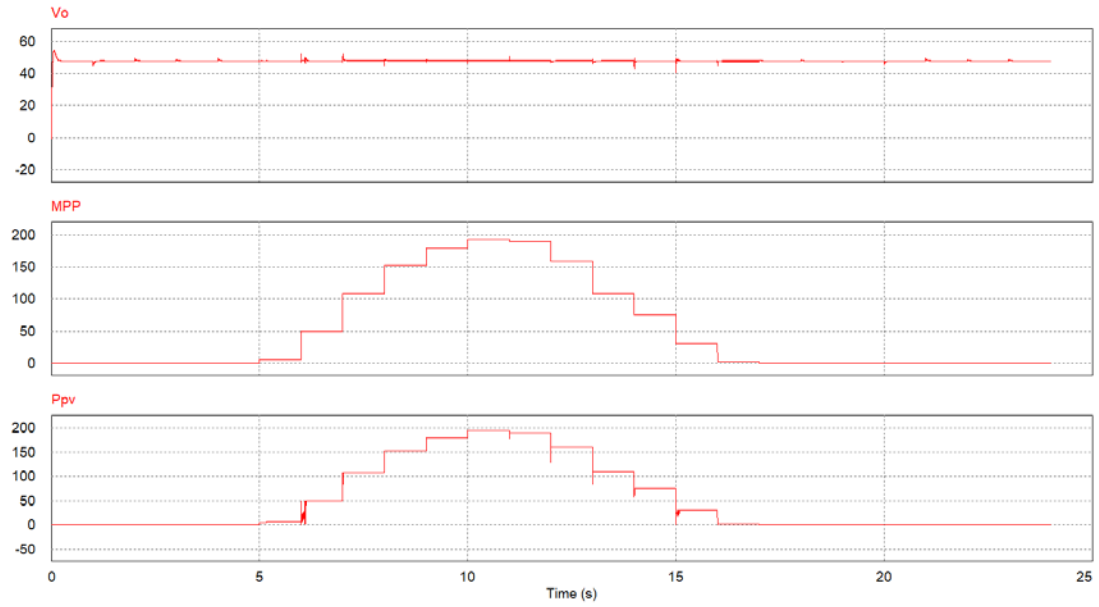

Figure 4.10: DC bus voltage (V_o), exact Maximum power available (MPP), and measured MPP (P_{pv}) from PSIM simulation for Zimbabwe

Figure 4.11 depicts the energy generation and consumption of the PV source, the battery, and the load. The PV source generates 1.25 kWh of energy, while the load consumes 1.1 kW. Meanwhile, the battery shows a net energy of -52 Wh. To calculate the energy efficiency of the system, we combine the total energy consumed by the load with the surplus energy gained by the battery. This sum represents the total output energy of the system. On the other hand, the energy generated by the PV source serves as the input energy for the system.

$$E_{eff} = \frac{E_o}{E_i} = \frac{1.1\times10^3 + 52}{1.25\times10^3} = 0.9216 \cong 92\% \qquad (4.1)$$

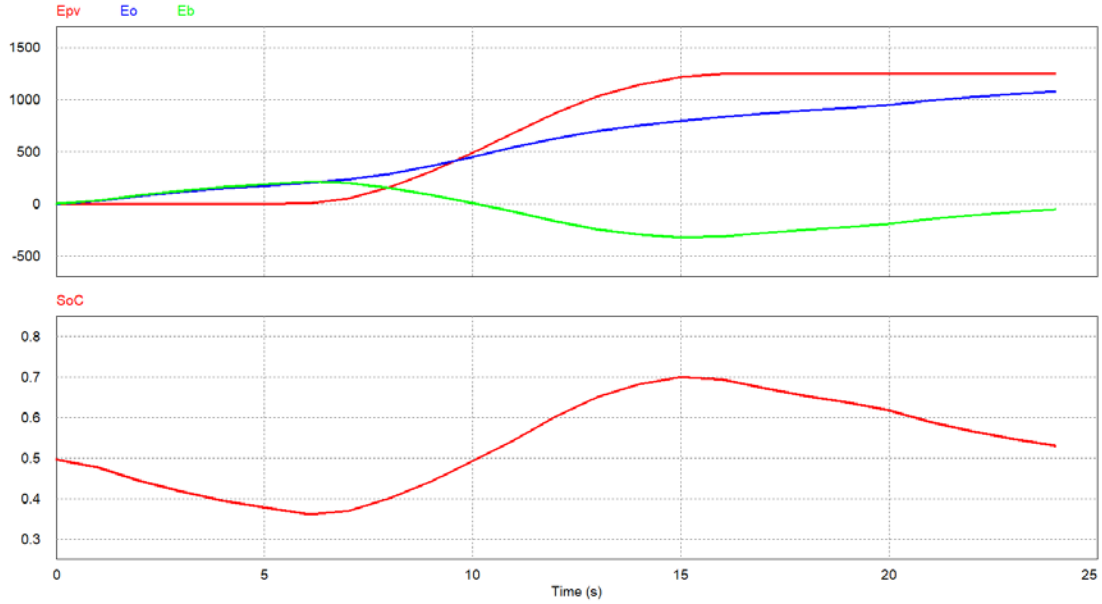

Figure 4.11: The energy generation and consumption by the PV source, battery, and load from PSIM simulation for Zimbabwe

4.5 Case Study II: Two load profiles

Providing two output voltage levels (12V and 48V) will not only minimize losses within the system but also provide a range of options for electrical appliances in off-grid communities. The 12V voltage level stands as the most compatible option for numerous electrical appliances and is widely used. Directly obtaining this voltage level from the battery significantly reduces losses that occur within the converter when bucking or boosting the voltage. However, high-power electrical appliances are experiencing substantial losses at 12V level. Additionally, many of these appliances are not available at 12V. Therefore, the inclusion of a 48V DC bus becomes essential to supply those loads when needed.

The primary objectives of this case study will remain the same as the previous one, with an additional focus on evaluating the reduction of losses when using both voltage levels (12V & 48V). Figure 4.12 shows the proposed TPC with load profiles connected at both voltage levels.

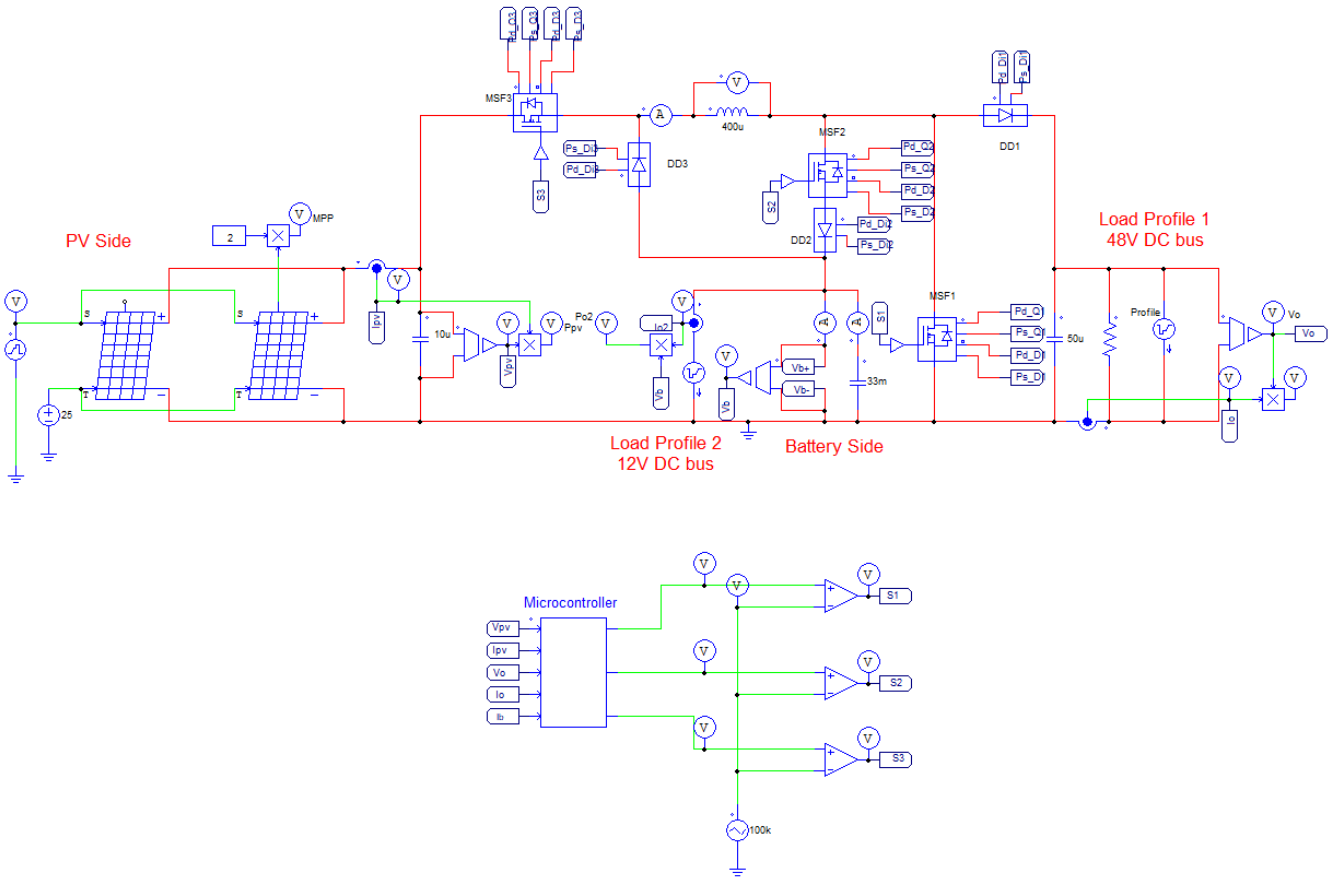

Figure 4.12: The proposed TPC with load profiles connected at both voltage levels

Figure 4.13 displays the two output voltage levels (V_o & V_b), the two load profiles (P_o & P_{o2}), and solar insolation profile (irradiance) from PSIM simulation for Zimbabwe.

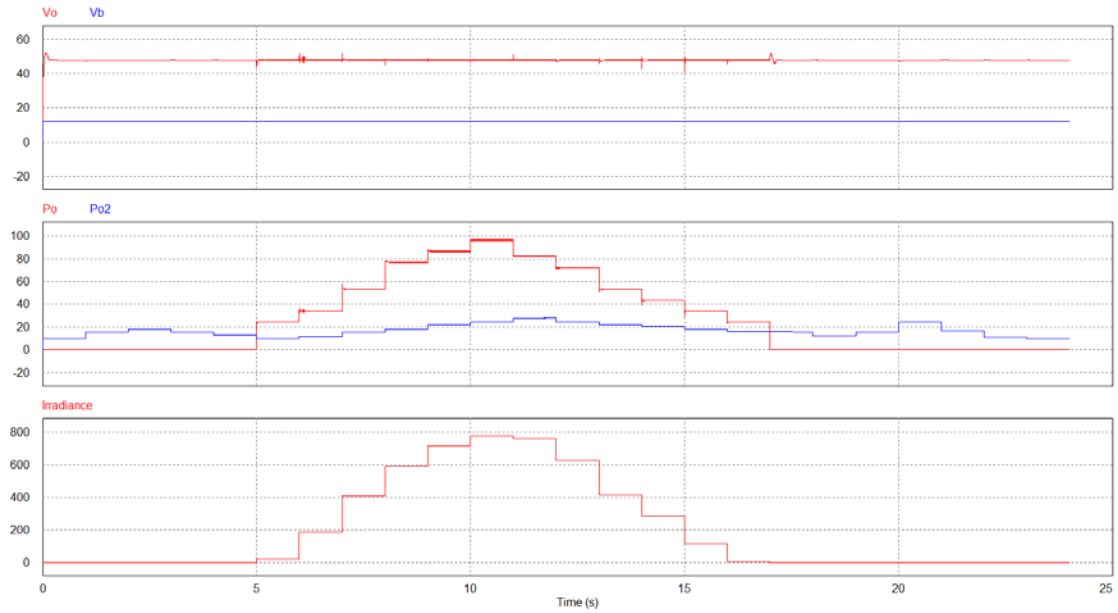

Figure 4.13: the two output voltage levels (V_o & V_b), the two load profiles (P_o & P_{o2}), and solar insolation profile (irradiance) from PSIM simulation for Zimbabwe

Figure 4.14 depicts the two output voltage levels (V_o & V_b), the PV power (P_{pv}) and the two load profiles (P_o and P_{o2}), and the battery current (I_b) from PSIM simulation. Battery is charging or discharging based on the power generated by the PV source and the power consumed by the two load profiles. It can be seen from the figure that when the power generated by the PV source is higher than the power consumed by the two load profiles, the battery is charging. In contrast, when the power generated by the PV source is lower than the power consumed by the two load profiles, the battery is discharging.

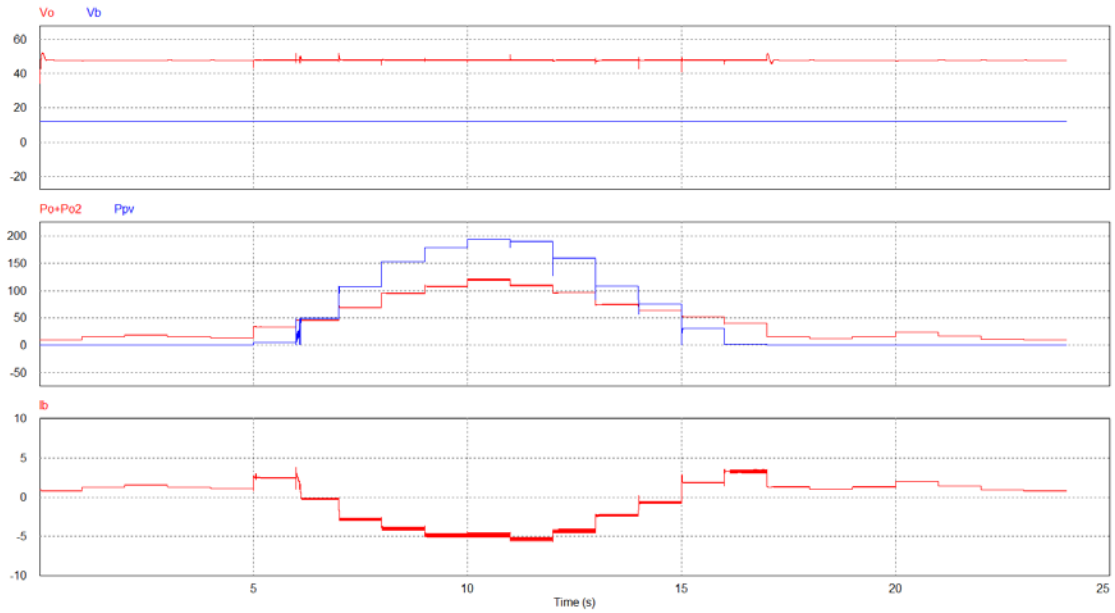

Figure 4.14: The two voltage levels (V_o & V_b), the PV power (P_{pv})and load profiles (P_o, & P_{o2}), and the battery current from PSIM simulation for Zimbabwe

Figure 4.15 depicts the energy generation and consumption of the PV source, the battery, and the load. The PV source generates 1.25 kWh of energy, while the load consumes 1.1 kW. Meanwhile, the battery shows a net energy of -71 Wh. To calculate the energy efficiency of the system, we combine the total energy consumed by the two loads with the surplus energy gained by the battery. This sum represents the total output energy of the system. On the other hand, the energy generated by the PV source serves as the input energy for the system.

$$E_{eff} = \frac{E_o}{E_i} = \frac{1.1\times10^3 + 71}{1.25\times10^3} = 0.9368 \cong 94\% \qquad (4.2)$$

By comparing the energy efficiencies of the two case studies, it can be seen that having two voltage levels improved the efficiency from 92% to 94%.

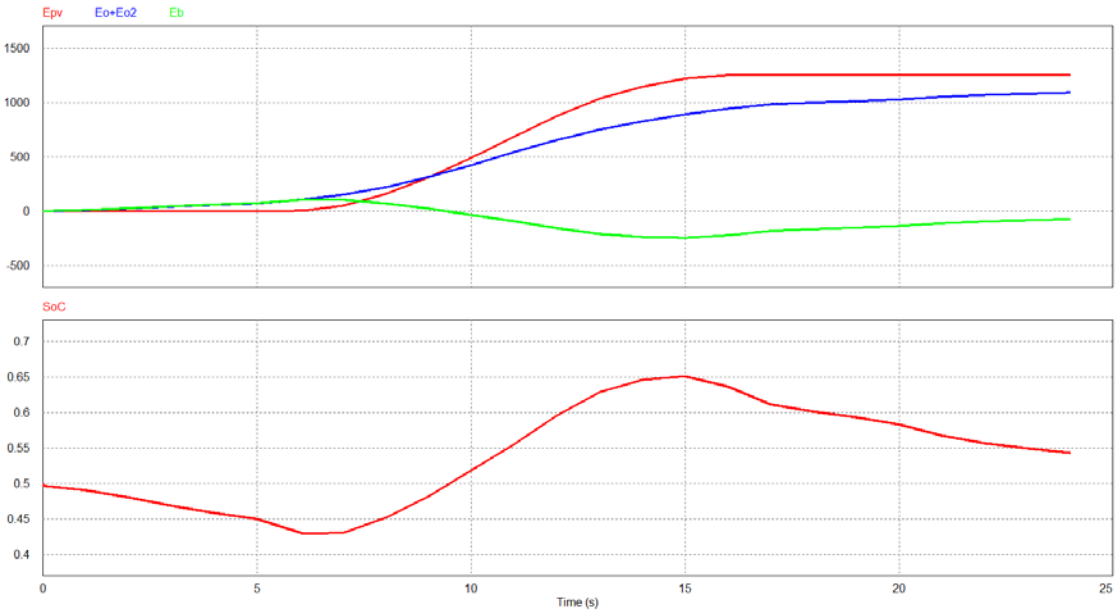

Figure 4.15: The energy generation and consumption by the PV source, battery, and load demand from PSIM simulation for Zimbabwe

4.6 Summary

In this chapter, a simulation analysis was conducted in PSIM software for the proposed topology. In section 4.1, the modes of operation were determined through comprehensive testing for various scenarios. In section 4.2, the proposed topology was evaluated for mode transition during operation. In section 4.3, different modes with different range of loads were tested to calculate the efficiency of the design. In section 4.4, a case study was conducted for a load profile at the 48V DC bus over a 24-hour period using PSIM. In section 4.5, another case study was conducted for two load profiles at the two output voltage levels (12V & 48V) over a 24-hour period.

Chapter 5
Conclusion and Future Work

5.1 Summary and conclusion

In this thesis, a novel three-port DC/DC Converter (TPC) for a small-scale standalone PV-Battery applications was proposed. This design targets underserved populations who reside in off-grid communities and are disconnected from centralized electricity grids. The design featured cost-effective design, reliable performance, two output voltage levels, and enhanced efficiency.

The derivation process of the topology and the optimization methodology were comprehensively presented to demonstrate the approach employed to develop the proposed design. The sharing of components across the different converters was maximized in order to reduce the components count. Moreover, the modes of operation were explained in detail to demonstrate the functionality of the TPC in the three modes: DO mode, DI mode, and SISO mode. To size the system, a load profile specific to an individual household in Zimbabwe was chosen from the existing literature. The goal was to meet the load requirement on an instantaneous basis in terms of stability and reliability, while adhering to the limitations of the renewable energy source, energy storage system, and other system components.

The control unit and the mode selection flow chart was thoroughly explained. The modes of operation of the TPC were determined by the available solar power, the load demand, and the battery SoC. A nested Proportional-Integral (PI) control loop was employed in order to regulate the output load voltage during load changes and the battery current during both charging and discharging to prevent exceeding the battery's limitations. For the PV port, the Maximum Power Point Tracking (MPPT) technique was employed using the Perturb and Observe (P&O) algorithm to ensure optimal power extraction from the solar panels.

The performance of the proposed topology was assessed using PSIM software. A comprehensive simulation analysis was conducted for a load profile over a 24-hour period. The steady-state waveforms for all the modes and the mode transition waveforms were all presented and discussed. Furthermore, the power efficiency for the proposed design was calculated for different range of loads and compared with other topologies. Finally, two case studies were presented to observe and analyze the system's response to different scenarios during the 24-hour period. Additionally, the improvements of having two output voltage levels on the overall losses of the design were presented and explained.

5.2 Contributions

The main contribution of the work reported in this thesis is the development of a novel three-port DC/DC converter (TPC) with low component count, high efficiency, low complexity, and two load ports at two different regulated voltages to serve both low-power and high-power applications in a home, in a remote off-grid community, under variable solar irradiance level and load demand.

5.3 Future Work

The system performs very well using PSIM software. However, there are some limitations in the simulations that prevented us from evaluating the performance of the proposed design further.

One of the limitations is the types of loads used across the DC bus. For instance, in order to simulate a load profile over a 24-hours period, a piecewise current source was used as a load. This was the only option in PSIM to assess the proposed design. However, to further evaluate the proposed design and its capability to regulate the voltage, it should be tested on different DC electronics loads, including but not limited to constant current (CC) loads, constant voltage (CV) loads, constant resistance (CR) loads, and constant power (CP) loads.

Another limitation is the ideality of the components used in PSIM software. To evaluate the efficiency of the design, thermal modules for the MOSFETs and diodes were only used. Therefore, a lab prototype is required to further assess the performance of the proposed design experimentally and measure the accurate efficiency of the system. This practical approach will enable validation of simulation findings, refining the design, and ultimately enhancing the performance and reliability of our system.

References

[1] IEA (2020), World Energy Outlook 2020, IEA, Paris https://www.iea.org/reports/world-energy-outlook-2020.

[2] Pachauri, S., Brew-Hammond, A., Barnes, D., Bouille, D., Gitonga, S., Modi, V., . . . Sathaye, J. (2012). Energy Access for Development. In Global Energy Assessment Writing Team (Author), Global Energy Assessment: Toward a Sustainable Future (pp. 1401-1458). Cambridge: Cambridge University Press. doi:10.1017/CBO9780511793677.025.

[3] H. Behjati and A. Davoudi, “Single-stage multi-port DC-DC converter topology,” IET Power Electron., vol. 6, no. 2, pp. 392–403, 2013.

[4] Neng Zhang, Danny Sutanto, Kashem M. Muttaqi, “A review of topologies of three-port DC–DC converters for the integration of renewable energy and energy storage system,” in Renewable and Sustainable Energy Reviews, Volume 56, 2016, Pages 388-401, ISSN 1364-0321,

[5] Q. Tian, G. Zhou, R. Liu, X. Zhang, and M. Leng, “Topology synthesis of a family of integrated three-port converters for renewable energy system applications,” IEEE Trans. Ind. Electron., vol. 68, no. 7, pp. 5833–5846, Jul. 2021.

[6] T. Cheng, D. D.-C. Lu, and L. Qin, “Non-isolated single-inductor DC/DC converter with fully reconfigurable structure for renewable energy applications,” IEEE Trans. Circuits Syst. II, Exp. Briefs, vol. 65, no. 3, pp. 351–355, Mar. 2018.

[7] Z. Qian, O. Abdel-Rahman, H. Hu and I. Batarseh, "An integrated three-port inverter for stand-alone PV applications," 2010 IEEE Energy Conversion Congress and Exposition, Atlanta, GA, USA, 2010, pp. 1471-1478, doi: 10.1109/ECCE.2010.5618252.

[8] H. Wu, R. Chen, J. Zhang, Y. Xing, H. Hu and H. Ge, "A Family of Three-Port Half-Bridge Converters for a Stand-Alone Renewable Power System," in IEEE Transactions on Power Electronics, vol. 26, no. 9, pp. 2697-2706, Sept. 2011, doi: 10.1109/TPEL.2011.2125991.

[9] Z. Qian, O. Abdel-Rahman, H. Al-Atrash and I. Batarseh, "Modeling and Control of Three-Port DC/DC Converter Interface for Satellite Applications," in IEEE Transactions on Power Electronics, vol. 25, no. 3, pp. 637-649, March 2010, doi: 10.1109/TPEL.2009.2033926.

[10] W. Jiang and B. Fahimi, "Multiport Power Electronic Interface—Concept, Modeling, and Design," in IEEE Transactions on Power Electronics, vol. 26, no. 7, pp. 1890-1900, July 2011, doi: 10.1109/TPEL.2010.2093583.

[11] A. Kwasinski, "Quantitative Evaluation of DC Microgrids Availability: Effects of System Architecture and Converter Topology Design Choices," in IEEE Transactions on Power Electronics, vol. 26, no. 3, pp. 835-851, March 2011, doi: 10.1109/TPEL.2010.2102774.

[12] J. L. Duarte, M. Hendrix and M. G. Simoes, "Three-Port Bidirectional Converter for Hybrid Fuel Cell Systems," in IEEE Transactions on Power Electronics, vol. 22, no. 2, pp. 480-487, March 2007, doi: 10.1109/TPEL.2006.889928.

[13] F. Z. Peng, Hui Li, Gui-Jia Su and J. S. Lawler, "A new ZVS bidirectional DC-DC converter for fuel cell and battery application," in IEEE Transactions on Power Electronics, vol. 19, no. 1, pp. 54-65, Jan. 2004, doi: 10.1109/TPEL.2003.820550.

[14] S. Harb, H. Hu, N. Kutkut, I. Batarseh and Z. J. Shen, "A three-port Photovoltaic (PV) micro-inverter with power decoupling capability," 2011 Twenty-Sixth Annual IEEE Applied Power Electronics Conference and Exposition (APEC), Fort Worth, TX, USA, 2011, pp. 203-208, doi: 10.1109/APEC.2011.5744598.

[15] A. K. Bhattacharjee, N. Kutkut and I. Batarseh, "Review of Multiport Converters for Solar and Energy Storage Integration," in IEEE Transactions on Power Electronics, vol. 34, no. 2, pp. 1431-1445, Feb. 2019, doi: 10.1109/TPEL.2018.2830788.

[16] Haimin Tao, J. L. Duarte and M. A. M. Hendrix, "Multiport converters for hybrid power sources," 2008 IEEE Power Electronics Specialists Conference, Rhodes, Greece, 2008, pp. 3412-3418, doi: 10.1109/PESC.2008.4592483.

[17] K. Sun, L. Zhang, Y. Xing and J. M. Guerrero, "A Distributed Control Strategy Based on DC Bus Signaling for Modular Photovoltaic Generation Systems With Battery Energy Storage," in IEEE Transactions on Power Electronics, vol. 26, no. 10, pp. 3032-3045, Oct. 2011, doi: 10.1109/TPEL.2011.2127488.

[18] S. Malo and R. Grino, “Design, construction, and control of a stand-alone energy-conditioning system for PEM-type fuel cells,” IEEE Trans. Power Electron., vol. 25, no. 10, pp. 2496–2506, Oct. 2010.

[19] Y. -C. Liu and Y. -M. Chen, "A Systematic Approach to Synthesizing Multi-Input DC–DC Converters," in IEEE Transactions on Power Electronics, vol. 24, no. 1, pp. 116-127, Jan. 2009, doi: 10.1109/TPEL.2008.2009170.

[20] Y. Li, X. Ruan, D. Yang, F. Liu and C. K. Tse, "Synthesis of Multiple-Input DC/DC Converters," in IEEE Transactions on Power Electronics, vol. 25, no. 9, pp. 2372-2385, Sept. 2010, doi: 10.1109/TPEL.2010.2047273.

[21] Y. Yuanmao and K. W. E. Cheng, "Level-Shifting Multiple-Input Switched-Capacitor Voltage Copier," in IEEE Transactions on Power Electronics, vol. 27, no. 2, pp. 828-837, Feb. 2012, doi: 10.1109/TPEL.2011.2155672.

[22] F. Nejabatkhah, S. Danyali, S. H. Hosseini, M. Sabahi and S. M. Niapour, "Modeling and Control of a New Three-Input DC–DC Boost Converter for Hybrid PV/FC/Battery Power System," in IEEE Transactions on Power Electronics, vol. 27, no. 5, pp. 2309-2324, May 2012, doi: 10.1109/TPEL.2011.2172465.

[23] C. N. Onwuchekwa and A. Kwasinski, "A Modified-Time-Sharing Switching Technique for Multiple-Input DC–DC Converters," in IEEE Transactions on Power Electronics, vol. 27, no. 11, pp. 4492-4502, Nov. 2012, doi: 10.1109/TPEL.2011.2180740.

[24] H. Wu, K. Sun, S. Ding and Y. Xing, "Topology Derivation of Nonisolated Three-Port DC–DC Converters From DIC and DOC," in IEEE Transactions on Power Electronics, vol. 28, no. 7, pp. 3297-3307, July 2013, doi: 10.1109/TPEL.2012.2221746.

[25] H. Zhang, D. Dong, M. Jing, W. Liu and F. Zheng, "Topology Derivation of Multiple-Port DC–DC Converters Based on Voltage-Type Ports," in IEEE Transactions on Industrial Electronics, vol. 69, no. 5, pp. 4742-4753, May 2022, doi: 10.1109/TIE.2021.3078389.

[26] R. Cheraghi, E. Adib and M. S. Golsorkhi, "A Nonisolated High Step-Up Three-Port Soft-Switched Converter With Minimum Switches," in IEEE Transactions on Industrial Electronics, vol. 68, no. 10, pp. 9358-9365, Oct. 2021, doi: 10.1109/TIE.2020.3026306.

[27] M. R. Al-Soeidat, H. Aljarajreh, H. A. Khawaldeh, D. D. -C. Lu and J. Zhu, "A Reconfigurable Three-Port DC–DC Converter for Integrated PV-Battery System," in IEEE Journal of Emerging and Selected Topics in Power Electronics, vol. 8, no. 4, pp. 3423-3433, Dec. 2020, doi: 10.1109/JESTPE.2019.2941595.

[28] R. Faraji, L. Ding, T. Rahimi, M. Kheshti and M. R. Islam, "Soft-Switched Three-Port DC-DC Converter With Simple Auxiliary Circuit," in IEEE Access, vol. 9, pp. 66738-66750, 2021, doi: 10.1109/ACCESS.2021.3076183.

[29] B. Chandrasekar et al., "Non-Isolated High-Gain Triple Port DC–DC Buck-Boost Converter With Positive Output Voltage for Photovoltaic Applications," in IEEE Access, vol. 8, pp. 113649-113666, 2020, doi: 10.1109/ACCESS.2020.3003192.

[30] F. Kardan, R. Alizadeh and M. R. Banaei, "A New Three Input DC/DC Converter for Hybrid PV/FC/Battery Applications," in IEEE Journal of Emerging and Selected Topics in Power Electronics, vol. 5, no. 4, pp. 1771-1778, Dec. 2017, doi: 10.1109/JESTPE.2017.2731816.

[31] K. Varesi, S. Hossein Hosseini, M. Sabahi, E. Babaei, S. Saeidabadi and N. Vosoughi, "Design and Analysis of a Developed Multiport High Step-Up DC–DC Converter With Reduced Device Count and Normalized Peak Inverse Voltage on the Switches/Diodes," in IEEE Transactions on Power Electronics, vol. 34, no. 6, pp. 5464-5475, June 2019, doi: 10.1109/TPEL.2018.2866492.

[32] R. Faraji and H. Farzanehfard, "Soft-Switched Nonisolated High Step-Up Three-Port DC–DC Converter for Hybrid Energy Systems," in IEEE Transactions on Power Electronics, vol. 33, no. 12, pp. 10101-10111, Dec. 2018, doi: 10.1109/TPEL.2018.2791840.

[33] B. R. Ravada, N. R. Tummuru and B. N. L. Ande, "Photovoltaic-Wind and Hybrid Energy Storage Integrated Multi-Source Converter Configuration for DC Microgrid Applications," in IEEE Transactions on Sustainable Energy, vol. 12, no. 1, pp. 83-91, Jan. 2021, doi: 10.1109/TSTE.2020.2983985.

[34] L. -J. Chien, C. -C. Chen, J. -F. Chen and Y. -P. Hsieh, "Novel Three-Port Converter With High-Voltage Gain," in IEEE Transactions on Power Electronics, vol. 29, no. 9, pp. 4693-4703, Sept. 2014, doi: 10.1109/TPEL.2013.2285477.

[35] Y. -M. Chen, A. Q. Huang and X. Yu, "A High Step-Up Three-Port DC–DC Converter for Stand-Alone PV/Battery Power Systems," in IEEE Transactions on Power Electronics, vol. 28, no. 11, pp. 5049-5062, Nov. 2013, doi: 10.1109/TPEL.2013.2242491.

[36] Rasoul Faraji, Ehsan Adib, Hosein Farzanehfard, “Soft-switched non-isolated high step-up multi-port DC-DC converter for hybrid energy system with minimum number of switches,” in

International Journal of Electrical Power & Energy Systems, Volume 106, 2019, Pages 511-519, ISSN 0142-0615, https://doi.org/10.1016/j.ijepes.2018.10.038.

[37] Prinsloo, Gerro, Dobson, Robert, & Brent, Alan. (2016). Scoping exercise to determine load profile archetype reference shapes for solar co-generation models in isolated off-grid rural African villages. Journal of Energy in Southern Africa, 27(3), 11-27. Retrieved July 29, 2023, from http://www.scielo.org.za/scielo.php?script=sci_arttext&pid=S1021-447X2016000300002&lng=en&tlng=en.

[38] Stackhouse, P. (n.d.). NASA POWER | Prediction Of Worldwide Energy Resources. https://power.larc.nasa.gov/

[39] M. Chen and G. A. Rincon-Mora, "Accurate electrical battery model capable of predicting runtime and I-V performance," in IEEE Transactions on Energy Conversion, vol. 21, no. 2, pp. 504-511, June 2006, doi: 10.1109/TEC.2006.874229.

[40] Power Electronics and Motor Drive Software | Altair PSIM. (n.d.). Default. https://altair.com/psim?utm_source=google-ads&utm_medium=cpc&utm_campaign=CORP-2023-PSIM-Search-Ads&utm_source=google&utm_medium=cpc&utm_campaign=&utm_term=psim&utm_content=-&hsa_acc=4984252251&hsa_cam=20338177614&hsa_grp=151790952620&hsa_ad=664769607295&hsa_src=g&hsa_tgt=kwd-430539297357&hsa_kw=psim&hsa_mt=p&hsa_net=adwords&hsa_ver=3&gad=1&gclid=CjwKCAjw8symBhAqEiwAaTA__POZ8yPCHJB6-hplyx4tPyLJIgi_aRDeolHMLqIdlTzbS06qs-qV2BoCuKgQAvD_BwE

Appendix A
Design of TPC

Because the load is changing, a load profile with variation in the range, 25W – 100W, was considered.

For $P_{low\ load} = 25\ W$

$$R_{low\ load} = \frac{V_o^{\ 2}}{P_{out}} = \frac{48^2}{25} = 92.16\Omega \quad \text{(A.1)}$$

For $P_{high\ Load} = 100\ W$

$$R_{\text{high } load} = \frac{V_o^{\ 2}}{P_{out}} = \frac{48^2}{100} = 23.04\Omega \quad \text{(A.2)}$$

A.1 PV to Load Path:

Because the voltage is step-up from the PV source to the load, the equations of a conventional boost converter was used.

To size the Inductor, first we need to calculate the duty cycle.

$$d = \frac{V_o - V_i}{V_o} = \frac{48-18}{48} = 0.625 \quad \text{(A.3)}$$

The relative current ripple of the inductor is chosen to be 20%.

For low power load:

$$L_{low\ power} = \frac{R_{low\ power} d(1-d)^2}{\frac{\Delta I_L}{I_L} f_s} = \frac{92.16 \times 0.625 \times (1-0.625)^2}{0.2 \times 100 \times 10^3} = 405\mu H \quad \text{(A.4)}$$

For high power load:

$$L_{high\ power} = \frac{R_{\text{high } power} d(1-d)^2}{\frac{\Delta I_L}{I_L} f_s} = \frac{23.04 \times 0.625 \times (1-0.625)^2}{0.2 \times 100 \times 10^3} = 101.25 \mu H \quad \text{(A.5)}$$

To size the capacitor, The relative voltage ripple is chosen to be 1%.

For low Power:

$$C_{low\ power} = \frac{d}{\frac{\Delta V_1}{V_1} R_{low\ power} f_s} = \frac{0.625}{0.01 \times 92.16 \times 100 \times 10^3} = 6.78 \mu F \quad \text{(A.6)}$$

For high Power:

$$C_{\text{high } power} = \frac{d}{\frac{\Delta V_1}{V_1} R_{low\ power} f_s} = \frac{0.625}{0.01 \times 23.04 \times 100 \times 10^3} = 27.13 \mu F \quad \text{(A.7)}$$

A.2 Battery to Load Path:

Because the path from the battery to the load is like a boost converter. Equations of a conventional boost converter are used,

To size the Inductor, first we need to calculate the duty cycle.

$$d = \frac{V_o - V_i}{V_o} = \frac{48-12}{48} = 0.75 \quad \text{(A.8)}$$

For low Power:

$$L_{low\ power} = \frac{R_{low\ power} d(1-d)^2}{\frac{\Delta I_L}{I_L} f_s} = \frac{92.16 \times 0.75 \times (1-0.75)^2}{0.2 \times 100 \times 10^3} = 216 \mu H \quad \text{(A.9)}$$

For high Power:

$$L_{high\ power} = \frac{R_{\text{high power}} d(1-d)^2}{\frac{\Delta I_L}{I_L} f_s} = \frac{23.04 \times 0.75 \times (1-0.75)^2}{0.2 \times 100 \times 10^3} = 54\mu H \quad \text{(A.10)}$$

To size the capacitor,

For low Power:

$$C_{low\ power} = \frac{d}{\frac{\Delta V_1}{V_1} R_{low\ power} f_s} = \frac{0.75}{0.01 \times 92.16 \times 100 \times 10^3} = 8.14\mu F \quad \text{(A.11)}$$

For high Power:

$$C_{high\ power} = \frac{d}{\frac{\Delta V_1}{V_1} R_{low\ power} f_s} = \frac{0.75}{0.01 \times 23.04 \times 20 \times 10^3} = 32.55\mu F \quad \text{(A.12)}$$

To ensure a relative current ripple for the inductor at 20% and relative voltage ripple for the capacitor at 1% over the entire load range, the following sizes were selected for L and C_o.

$$L = 400\mu H$$
$$C_o = 50\mu F$$

Appendix B

C- Code for the controller

```
Vpv=in[0];
Ipv=in[1];
Vo=in[2];
Io=in[3];
Ib=in[4];

Ppv=Vpv*Ipv;
Po=Vo*Io;

//////*MPPT Code Starts*//////

DeltaVpv=Vpv-Vpv_prev;
DeltaPpv=Ppv-Ppv_prev;

if (DeltaPpv>0){
    if (DeltaVpv>0){
        D=D-step;
    }
    else if (DeltaVpv<0){
        D=D+step;
    }
}
else if (DeltaPpv<0){
    if (DeltaVpv<0){
        D=D-step;
    }
    else if (DeltaVpv>0){
        D=D+step;
    }
}

if (D>Dmax){
    D=Dmax;
}
else if (D<Dmin){
    D=Dmin;
}

Vpv_prev=Vpv;
Ppv_prev=Ppv;

IVR=D;

//////*MPPT Code Ends*//////


if (Ppv>0)
```

```
{
    if (Ppv>Po)
    {

        //////*PI Controller For Voltage Starts*//////

        double kp =2;
        double ki = 0.00002;


        error = vref - Vo;

        integral = integral + error*ki + errorprev*ki;

        errorprev = error;

        I_b = (error*kp) + integral;

        //////*PI Controller For Voltage Ends*//////


        //////*PI Controller For Current Starts*//////

        double kp2 = 0.02;
        double ki2 =  0.000002;


        error2 = I_b - Ib;

        integral2 = integral2 + error2*ki2 + errorprev2*ki2;

        errorprev2 = error2;

        OVR = (error2*kp2) + integral2;

        if ( OVR>0.85)
        OVR = 0.85;
        if (OVR<0)
        OVR = 0;

        //////*PI Controller For Current Ends*//////

        out[0]=OVR;
        out[1]=IVR ;
        out[2]=1;
    }

    else if (Ppv<Po)
    {

        //////*PI Controller For Voltage Starts*//////
```

```
        double kp =1;
        double ki =0.00005;

        error = vref - Vo;

        integral = integral + error*ki + errorprev*ki;

        errorprev = error;

        I_b = (error*kp) + integral;

        //////*PI Controller For Voltage Ends*//////


        //////*PI Controller For Current Starts*//////

        double kp2 = 0.1;
        double ki2 = 0.000005;


        error2 = I_b - Ib;

        integral2 = integral2 + error2*ki2 + errorprev2*ki2;

        errorprev2 = error2;

        OVR = (error2*kp2) + integral2;

        if ( OVR>0.85)
        OVR = 0.85;
        if (OVR<0)
        OVR = 0;

        //////*PI Controller For Current Ends*//////

        out[0]=OVR;
        out[1]= 0;
        out[2]=IVR;
    }
}
else if  (Ppv<=0)
    {

        //////*PI Controller For Voltage Starts*//////

        double kp =1.2;
        double ki = 0.00001;


        error = vref - Vo;

        integral = integral + error*ki + errorprev*ki;
```

```
    errorprev = error;

    I_b = (error*kp) + integral;

    //////*PI Controller For Voltage Ends*//////


    //////*PI Controller For Current Starts*//////

    double kp2 =0.05;
    double ki2 = 0.000001;


    error2 = I_b - Ib;

    integral2 = integral2 + error2*ki2 + errorprev2*ki2;

    errorprev2 = error2;

    OVR = (error2*kp2) + integral2;

    if ( OVR>0.85)
    OVR = 0.85;
    if (OVR<0)
    OVR = 0;

    //////*PI Controller For Current Ends*//////

    out[0]=OVR;
    out[1]= 0;
    out[2]=0;
}
```